

Published as: Collins, A.S., Reddy, S.M., Buchan, C and Mruma, A. 2004. Temporal Constraints on Palaeoproterozoic Eclogite Formation and Exhumation. *Earth and Planetary Science Letters*, 224, 177-194.

Temporal Constraints on Palaeoproterozoic Eclogite Formation and Exhumation (Usagaran Orogen, Tanzania)

**Alan S. Collins^{1,2*}, Steven M. Reddy¹, Craig Buchan¹
and Abdul Mruma³**

¹*Tectonics SRC, Department of Applied Geology, Curtin University of Technology, GPO
Box U1987, Perth WA 6845, Australia*

²*Present Address: Tectonics SRC, School of Earth and Geographical Sciences (M004),
The University of Western Australia, Crawley WA 6009, Australia*

³*Department of Geology, Dar es Salaam University, Dar es Salaam, Tanzania*

Keywords: eclogite, Palaeoproterozoic, SHRIMP, U-Pb isotopes, Usagaran Orogen,
exhumation, zircon, dating deformation, Tanzania, geochronology

Abstract

In-situ rock suites that preserve assemblages consistent with metamorphism to eclogite-facies conditions are absent from the Archaean. Their Palaeoproterozoic appearance is one of the markers of the onset of tectonic processes similar to those seen in the Phanerozoic Earth. We report new U-Pb SIMS zircon data from the oldest known eclogites (the ~2.0 Ga Usagaran eclogites, Tanzania) that constrain the timing of high-grade metamorphism, deformation and exhumation of these eclogites and constrain the speed of these processes at this critical period in Earth history.

Direct dating of metamorphic zircon from mafic eclogites, isostructurally recrystallised zircon rims from pelites and felsic gneisses indicates that high-grade metamorphism occurred at 1999.1 ± 1.1 Ma. The rocks were quickly cooled and exhumed at rates of $\sim 25^\circ\text{C}/\text{Ma}$ and $0.06\text{-}0.22$ GPa/Ma respectively, at least in part, by amphibolite-facies sinistral transpression that was sealed by a 1991 ± 2 Ma pegmatite dyke. Detrital zircons in the protolith were dominantly derived from two sources: 1) the Tanzanian craton, and; 2) a 2400-2640 Ma source region that is compatible with a belt of reworked Archaean and Palaeoproterozoic rocks that lie in the East African Orogen.

1. Introduction

In-situ (i.e. non-xenolithic) rocks older than 1500 Ma that preserve evidence of metamorphism at pressures >1.0 GPa are extremely rare (Fig. 1)[1]. Even more scarce are rocks of this antiquity that preserve evidence that they experienced eclogite-facies conditions. In a review of published examples, O'Brien and Rötzler [1] described only two examples, retrogressed ~ 1800 Ma eclogites in the Hengshan region of the North China Craton [2] and ~ 2000 Ma, near pristine, eclogites within the Ubendian/Usagaran Orogen (<1.8 GPa, $\sim 750^\circ\text{C}$)[3-5], which partly surrounds the Neoproterozoic Tanzanian craton, Fig. 2). In addition, 1905-1880 Ma marginal eclogites (~ 1.2 GPa and $650-700^\circ\text{C}$) have been reported from the Lapland Granulite Belt, Finland [6], ~ 1900 Ma retrogressed eclogites occur in the Aldan Shield, Siberia [7] and ~ 1900 Ma high-pressure granulites occur in the Snowbird tectonic zone between the Rae and Hearne cratons of Canada [8]. Of these, the Ubendian/Usagaran eclogites are the oldest and are the only examples to preserve pristine unequivocal eclogite-facies mineral assemblages [3].

Phanerozoic eclogite-facies rocks and high pressure granulites commonly preserve evidence of having been partially subducted to sub-crustal depths and rapidly exhumed along near-isothermal P-T paths [1, 9-12](Fig. 1). In the modern Earth, these unusual conditions are met in subduction-accretion complexes and sites of continental collision, where relatively cold crust is buried to depths greater than ~ 50 km. For these rocks to return to the Earth's surface with preserved eclogite-facies mineral assemblages requires rapid exhumation of the subduction complex [e.g. 9], before tectonically depressed isotherms can re-equilibrate and overprint eclogite assemblages with higher temperature granulite-facies minerals. The fundamental observation that Archaean eclogite-facies

rocks have not been found suggests that before Palaeoproterozoic times, either, the conditions to produce such rocks did not exist, the processes to exhume them at a sufficient rate to preserve eclogite-facies mineral assemblages did not exist, or, all pre-existing examples have been pervasively overprinted by subsequent tectonic events. Documenting the tectonic environment of metamorphism and process of incorporation into the host orogens of Palaeoproterozoic eclogites is therefore of considerable importance for understanding the evolution of tectonic processes.

In this paper we present Secondary Ion Microscopy (SIMS) U-Pb isotopic data from zircons obtained using the Sensitive High Resolution Ion Microprobe (SHRIMP). By integrating these age data with individual zircon textural characterisation, cathodoluminescence (CL) imaging, and detailed field mapping, we have been able to date high-grade metamorphism and tightly constrain deformation associated with emplacement and exhumation of the eclogite-facies rocks.

2. Regional Geology

The Usagaran Orogen of central Tanzania is a Palaeoproterozoic orogenic belt that lies directly southeast of the ~2.7 Ma Tanzanian Craton (Fig. 2). In the south, the 2.0 Ga Usagaran Orogen links with a similar sequence of rocks of the Ubendian Orogen of western Tanzania. To the east and north the Usagaran Orogen becomes progressively reworked in the East African Orogen; a zone of Neoproterozoic (620-690 Ma) [13, 14] orogenesis associated with the final amalgamation of Gondwana [15-17].

The Usagaran Orogen is subdivided into two major litho-tectonic units; the Konse Group and the Isimani Suite (Fig. 2b). The Konse Group [18, 19], formerly the Konse Series

[20, 21], is composed of a stratigraphic succession of seven sedimentary and volcanic formations subsequently metamorphosed at greenschist-facies conditions. At its base, the Konse Group unconformably overlies foliated rocks of both the Isimani Suite and the Tanzanian Craton [19, 20].

The Isimani Suite [19], lies to the east of the Konse Group and comprises numerous different rock types that record a range of different mineral assemblages indicating high-grade amphibolite, granulite and eclogite-facies metamorphism (Figs. 2b and 3). Peak eclogite-facies conditions are constrained at $\sim 750^{\circ}\text{C}$ and ~ 1.8 GPa [3]. Fluid inclusions preserve pressures indicative of being trapped under eclogite-facies conditions and independently support the petrologically derived pressure-temperature curve (Fig. 1)[5]. An isothermal decompression path was obtained by using the compositions of orthopyroxene + hornblende + plagioclase garnet coronas that yielded pressures of 0.9-1.0 GPa and temperatures of $665\text{-}780^{\circ}\text{C}$ [3]. An amphibolite-facies metamorphic event (0.4-0.6 GPa, $500\text{-}700^{\circ}\text{C}$)[19] overprinted these high pressure assemblages.

Isimani gneisses have been interpreted to have a sedimentary origin due to their lateral extent and the presence of kyanite-bearing mica schists [19], although a 2705 ± 11 Ma orthogneiss component was identified by Reddy et al. [22]. Mafic rocks have been inferred to be of magmatic origin [19] and trace and rare-earth element geochemistry has been used to infer a MORB-type protolith [3].

A recently published structural analysis of the Isimani Suite by Reddy et al. [22] documented bulk D_2 sinistral transpression deformation during amphibolite-facies conditions that post-dated eclogite formation.

3. Previous Geochronology

Previous geochronological constraints on the timing of protolith formation, deformation and metamorphism within the Usagaran Orogen have highlighted the antiquity of the Usagaran protoliths and the importance of Palaeoproterozoic high-grade metamorphism. Depleted mantle Nd model ages of 2.7-3.1 Ga and U-Pb SIMS zircon ages of ~2.7 Ga obtained from Isimani felsic gneisses [22, 23] and 2.1-2.5 Ga Nd and Sr model ages from post-tectonic granites [24] suggest that a significant component of Archaean material is common throughout eastern Tanzania. Coupled thermo-barometric analysis and U-Pb monazite ages suggest that eclogite-facies (M_1) metamorphism took place at 1999.5 ± 1.4 Ma [3]. The Konse Group (Fig. 2) has been dated by correlation with the Ndembera volcanics of Tanzania [19, 20] from which whole rock Rb-Sr data yield an age of 1895 ± 27 Ma [age recalculated from 25, using the decay constant of, 26]. A U-Pb zircon ion-microprobe age of 1877 ± 7 Ma has been obtained from the post-tectonic Kidete Granite (Fig. 2b), which provides the lower constraint on high-grade deformation [22]. Rb/Sr biotite-whole rock isochrons on the Usagaran gneisses and post-tectonic granites yield ages ranging from 432 ± 5 Ma to 1956 ± 53 Ma [recalculated from 25] and K-Ar biotite ages from ~500-3200 Ma [25, 27]. Gabert and Wendt [27] noted that within this range there was a general southeastward younging in ages away from the Tanzanian craton, which they interpreted as resetting by a late Neoproterozoic thermal event associated with the East African Orogen. Laser $^{40}\text{Ar}/^{39}\text{Ar}$ data from muscovites are interpreted as cooling below $\sim 350^\circ\text{C}$, after a Neoproterozoic/Cambrian greenschist-facies metamorphic event that occurred throughout the Usagaran region, at, or after, 535.4 ± 2.3

Ma [28]. Discordant U-Pb rutile ages from retrogressed eclogite-facies rocks with a lower intercept of 501 ± 26 Ma [3] support the presence of a Neoproterozoic thermal overprint.

4. Analytical techniques

Zircons were separated from crushed rock samples by conventional magnetic and heavy liquid separation. Grains were handpicked and mounted in epoxy resin discs that were coated with a thin layer of gold. The crystals were then imaged using a CL detector fitted to a Phillips XL30 scanning electron microscope at a working distance of 15 mm and using an accelerating voltage of 10 kv.

Zircon U-Th-Pb isotopic data were collected using the Perth SHRIMP II. The sensitivity for Pb isotopes in zircon, with a primary beam current of 2.5-3.0 nA and mass resolution of ~ 5000 , was ~ 18 cps/ppm/nA,. Correction of measured isotopic ratios for common Pb was based on the measured ^{204}Pb in each sample and often represented a $<1\%$ correction to the ^{206}Pb counts (see %common ^{206}Pb in Table 1). The common Pb component, being largely surface contaminant, was modelled on the composition of Broken Hill ore Pb.

Pb/U isotopic ratios were corrected for instrumental inter-element discrimination using the observed covariation between Pb^+/U^+ and UO^+/U^+ [29, 30] determined from interspersed analyses of the Perth standard zircon CZ3, which is a single zircon megacryst from Sri Lanka with an age of 564 Ma and a $^{206}\text{Pb}/^{238}\text{U}=0.0914$ [31].

5. Sample and zircon characteristics

5.1. T01-02 - Biotite Leucocratic gneiss

This sample comes from the far east of our Great Ruaha River transect (36°10'54"E 07°09'12"S)(Fig. 2). The outcrop consists of biotite leucocratic gneiss that has a prominent mineral lineation defined by biotite aggregates and well foliated zones rich in muscovite.

The majority of zircons separated from T01-02 have prismatic habits with rounded pyramidal terminations. Their axial aspect ratios vary between 2:1 and 4:1 (Fig. 4a). These grains weakly luminesce and some preserve oscillatory zoning. Grain 12 (Fig. 4a) has an irregular, moderately luminescent partial rim that protrudes to the middle of the grain crosscutting poorly-imaged luminescent zones in the core of the grain. One grain (Grain 3, Fig. 4b) has a thick, brightly luminescent, rim with broad luminescent bands and cracks that radiate from a dark core. Approximately 40% of the separated grains have thin, brightly luminescent rims, or partial rims, of a couple of μm thick (e.g. Grain 3, Fig. 4b).

5.2. T01-05 - *Kyanite-Garnet Pelitic Gneiss*

This sample is from a large cliff on the north bank of the Great Ruaha River (36°09'28"E 07°09'00"S)(Fig. 2). The sample consists of kyanite, garnet, hornblende, biotite, quartz and plagioclase and is associated with garnet amphibolite boudins (Fig. 3a). The ubiquitous presence of kyanite and the micaceous nature of the rock suggest that the protolith was a pelitic sedimentary rock. These pelitic gneisses are intercalated with garnet amphibolite that correlates along strike with the Yalumba Hill mafic eclogite (Fig. 2b, Sample T01-40). The sample is well foliated with a prominent mineral lineation defined by aligned kyanite blades.

Zircons separated from this sample have heterogeneous morphologies from rounded, sub-equant to subhedral prismatic grains with aspect ratios of 4.5:1, however, all grains show some degree of rounding of crystal terminations. The majority of grains (~80%) have prominent cores in CL images (Fig. 4c-f) that are usually poorly luminescent. These cores preserve luminescence bands that are broadly parallel to one or more of the grain faces (Fig. 4c,d,e,f). The parallel banded core to Grain 08 (Fig. 4f) is overgrown by poorly luminescent oscillatory zoned zircon that is traced into the rim. The rims are defined by a marked change in luminescence intensity. This is commonly a change from poorly luminescent cores to brightly luminescent rims, but in Grain 03 (Fig. 4d) a poorly luminescent core is separated from a poorly luminescent rim by a strongly luminescent band. Oscillatory zoning in the rim is preserved in all of the presented examples (Fig. 4c-f), although in two of the examples (Fig. 4c,e) this regular banding is overprinted by zones of highly heterogeneous luminescence that are concentrated at the core/rim boundary. This boundary often broadly follows the grain margin, but can be highly irregular (Fig. 4e). Luminescence patterns in the core can sometimes be traced into the rim across the transgressive core/rim boundary (“x” in Fig 4f) and crystal-face parallel core luminescent bands pass through to the rim and define the outer shape of the crystal (Fig. 4e,f). These features suggest that the oscillatory zoned zircon in the core and rim of a number of grains (and especially Grain 8) formed together as primary precipitated zircon [32]. The blurring of the luminescent banding in the rims and the change in luminescence brightness suggest that secondary textures have overprinted primary core textures, similar to solid-state recrystallised rims [32, 33].

5.3. T01-12a - Pegmatite

T01-12a (36°09'04''E 07°08'57''S)(Fig. 2) is a sample of a 20-40 cm thick undeformed pegmatite that cuts through centimetre-scale S₂ tectonite bands in leucocratic gneiss and decimetre-scale amphibolite interlayers (Fig. 3b) with garnet pseudomorphs. The pegmatite cuts the steep limb of a F₃ fold. From the cross-cutting relationship and undeformed nature of the pegmatite, it is interpreted that the pegmatite post-dates D₂ mylonitic deformation and formed either during or after D₃ deformation.

Many zircons extracted from this sample preserve pristine euhedral prisms with pyramidal terminations (Fig. 5a). The grains commonly have an aspect ratio between 3:1 and 4:1. Euhedral zircons from this sample varied in size from 100-500 µm. A number of anhedral zircons also occur that have ovoid to circular morphologies. CL images highlight distinct brightly luminescent ovoid to rounded prismatic cores in many of the euhedral crystals that preserve sector and concentric luminescent zones. Where a core is present in the euhedral crystal a very poorly luminescent, near homogenous, rim surrounds it (Fig. 5b,c,d). A number of euhedral grains have no discernable core and all the anhedral grains preserve no rim, or only very thin (<5 µm) rims.

5.4. T01-19 - Blastomylonitic Felsic Gneiss

T01-19 (36°08'43''E 07°08'20''S)(Fig. 2) contains biotite, plagioclase and quartz, displays a mylonitic foliation and has a prominent mineral aggregate lineation on the foliation planes that is perpendicular to the macroscopic vorticity axis derived from excellent δ-type inclusions of quartz (Fig 3c).

Zircons extracted from T01-19 consist of rounded prismatic grains with cross-section aspect ratios of 3:1 to 4:1 and subhedral pyramidal terminations (Fig. 6a,b,c). CL images

illustrate common sector and oscillatory zoned cores. The oscillatory zoned examples preserve internal zone truncations (Fig. 6c) and in some cases the relative development of different crystal faces during growth (e.g. the development of pyramidal faces over the basal pinacoid in Fig. 6b). Homogenous brightly luminescent zircon patches overgrow some oscillatory zoning and are similar in appearance to the “zone controlled alteration” reported by Vavra et al. [34]. In both Grains 04 and 07 (Fig 6a,b) distinct cores with variable CL intensity are surrounded by rims that display broad luminescence banding (Rim 1 in Fig. 6b). Grains 07 and 11 (Fig. 6b,c) preserve poorly luminescent outer bands (Rim 2 in Fig. 6b) that have weak wispy textures. In Grain 11 (Fig. 6c) this outer rim is separated from the core by a bright luminescent band that truncates the core zoning. In Grain 07 (Fig. 6b) the outer rim (Rim 2) truncates the bands of the inner rim (Rim 1), with the boundary between them approximately parallel to the outer margin of the grain. Subhedral to anhedral grains occur in addition to prismatic grains. These grains have poor luminescence and textures are only observed when imaged with extreme contrast. In Grain 18 (Fig. 6d), weak oscillatory zoning is barely visible and the grain is partially rimmed by an extremely thin brightly luminescent band.

5.5 T01-40 – Mafic Eclogite

This sample was collected approximately half way up the north spur of Yalumba Hill (36°16'35``E 06°59'00``S)(Figs. 2 & 3d). The sample is from a massive metre- to ten metre-scale lens of garnet + omphacite + plagioclase rock surrounded by foliated and lineated garnet amphibolite. Garnets in the surrounding amphibolites locally preserve coronas of chlorite and actinolite and irregular patches occur where garnet has been completely pseudomorphed by aggregates of actinolite, quartz and chlorite.

The sample is rich in large (150-400 μm diameter) anhedral zircons. Figure 7 shows highly luminescent zircon regions (analyses labelled “light” in Table 1) separated from lower luminescent rims (analyses labelled “dark” in Table 1). Where both luminescence tones are present in the same grain, lighter luminescent zircon often forms distinct sector-zoned cores surrounded by darker-luminescent, relatively homogenous, rims (Fig. 7a-f). The rims often transgress the core (Fig. 7a, d) and in Grain 21 (Fig. 7a), replace brightly luminescent core zircon along individual planar oscillatory zones. In a number of grains two rims are distinguished, an inner one that preserves “ghost” luminescent patterns traceable from the core, and a thin homogenous outer rim (Fig 7e). A number of grains have a subhedral prismatic morphology (Fig. 7c) with faintly luminescent concentric zones preserved in the core similar to other high-pressure metamorphic zircons that have been interpreted as reflecting crystallisation in local melts or supercritical fluids at near-peak metamorphic conditions [35, 36].

6. U-Th-Pb SHRIMP results

6.1. U-Th-Pb Chemistry

Figure 8 comprises plots of U versus Th and $^{207}\text{Pb}/^{206}\text{Pb}$ age versus $^{232}\text{Th}/^{238}\text{U}$ ratio for each analysed sample (data in Table 1), with data subdivided into cores and rims based on CL images. Core analyses from the amphibolite-facies felsic gneiss samples (T01-02, T01-19) both preserve moderately high U and Th contents (U = 160-6000 ppm, Th = 28-2300 ppm) and have a wide range of $^{232}\text{Th}/^{238}\text{U}$ ratios spanning two orders of magnitude (0.01-1.7). Only two rims were analysed in T01-02 with one rim showing much lower U

abundances than the core. Rim analyses of T01-19 are markedly lower in Th than adjacent cores, but slightly higher in U with a resulting decrease in $^{232}\text{Th}/^{238}\text{U}$ ratio. A complication with this sample is the presence of multiple-stage rims on some of the zircon cores (see above). The $^{232}\text{Th}/^{238}\text{U}$ ratio falls to ≤ 0.2 in all but one case when rims with $^{207}\text{Pb}/^{206}\text{Pb}$ ages < 2010 Ma are considered.

Thorium contents in zircons analysed from the metasedimentary kyanite-garnet gneiss (T01-05) are extremely variable, spanning four orders of magnitude (0.03-634 ppm). Core analyses have similar contents to those zircons analysed in the felsic gneisses T01-02 and T01-19. In contrast, rim U and Th concentrations form a broad depletion trend from values similar to those of the cores, to extremely low Th values and less depleted U concentrations.

Zircons from the post-D2 pegmatite (T01-12a) show a similar decrease in $^{232}\text{Th}/^{238}\text{U}$ ratio between the cores and the euhedral rims. However, in contrast to the gneissic samples, this decrease is coupled by an absolute increase in U, and to a lesser extent, Th.

Th and U concentrations in zircons from the mafic eclogite sample (T01-40) span two orders of magnitude (U = 2-75 ppm, Th = 1-110 ppm) with a number of analyses yielding < 10 ppm of U and Th (Fig. 8 and Table 1). No definitive correlation between luminescence and U or Th content is apparent, but strongly-luminescent regions (“light” in Fig. 8), which commonly occur in the centre of grains and are rimmed by apparently later developed, poorly-luminescent, zircon (“dark” in Fig. 8), are generally poorer in both Th and U and preserve a higher $^{232}\text{Th}/^{238}\text{U}$ ratio (Fig. 8). The lowest concentrations of U and Th are found in zircon that displays the weakest luminescence (Figs. 7 and 8 and Table 1).

6.2. *U-Th-Pb Isotopic Ages*

U-Th-Pb isotopic data are presented in Table 1. Concordia plots are presented in Figure 9 and probability distribution plots of the >2050 Ma core analyses are presented in Figure 10.

6.2.1 T01-02 – Biotite Leucocratic gneiss

Isotopic analyses yield a spread of <10% discordant $^{207}\text{Pb}/^{206}\text{Pb}$ ages from 2561 ± 6 Ma to 2979 ± 9 Ma (1σ error)(Table 1, Fig. 9a). Two interpretations of the data are possible. Firstly, the spread of ages may indicate that the sample contains a temporally heterogeneous population of zircons that formed between 2555 and 2988 Ma. Secondly, the zircons may have formed at 2851 ± 110 Ma (the upper intercept of an imprecise discordia line, Fig. 9a) and then have lost varying amounts of Pb during an isotopic disturbance event at 2026 ± 110 Ma (lower discordia intercept). Evidence for a disturbance event includes the observation that in Grain 3 (Fig. 4b) the age of the rim is considerably older than that of the core, implying that in some grains at least the isotopic record has been disturbed. Also, the lower discordia intercept is geologically meaningful, being close to published estimates of the age of metamorphism of the Isimani Suite [3, 22]. Support for the first interpretation includes the observation that the most concordant analyses are spread over the full age range suggesting that the discordia may be an artefact and that the age range is similar to those of undisputed metasedimentary rocks (e.g. T01-05 below).

6.2.2 T01-05 – Kyanite-Garnet Gneiss

$^{207}\text{Pb}/^{206}\text{Pb}$ ages of zircon cores range from 2427 ± 15 Ma to 3022 ± 10 Ma (Fig. 9b). A probability distribution plot of these core ages has large peaks centred on 2580 and 2684 Ma (Fig. 10). A weighted mean of 25 zircon $^{207}\text{Pb}/^{206}\text{Pb}$ rim ages results in an age of 1989 ± 10 Ma (MSWD=0.56). Twenty one of these analyses have $^{232}\text{Th}/^{238}\text{U}$ ratios <0.1 .

6.2.3. T01-12a - Pegmatite

Zircon cores yield ages that congregate between 2480 ± 9 Ma and 2867 ± 30 Ma (1σ error) with one analysis providing a concordant age of 2099 ± 31 Ma (Fig. 9c). These analyses are interpreted as dating xenocrystic zircon inherited from the country rock. Weakly luminescent zircon rims have very low $^{232}\text{Th}/^{238}\text{U}$ ratios (≤ 0.01). Fourteen rim analyses give a weighted $^{207}\text{Pb}/^{206}\text{Pb}$ age of 1991 ± 2 Ma (MSWD = 0.79).

6.2.4. T01-19 – Blastomylonitic Felsic Gneiss

Zircon cores are concordant to strongly discordant ($<44\%$) and yield a spread of $^{207}\text{Pb}/^{206}\text{Pb}$ ages between 2489 ± 16 Ma and 2959 ± 4 Ma (1σ error)(Fig. 9d). The oldest age is from a zircon core that is rimmed with oscillatory zoned zircon that yielded a $^{207}\text{Pb}/^{206}\text{Pb}$ age of 2678 ± 5 Ma. This may date magmatic zircon crystallisation of this rim around a xenocryst. Uniform poorly luminescent zircon rims occur around a number of grains, which along with analyses of two grains of homogenous poorly luminescent crystals, have a weighted mean $^{207}\text{Pb}/^{206}\text{Pb}$ age of $1997.6 \pm 2/-2.2$ Ma (2σ error, 7 analyses, MSWD = 1.16). These younger analyses all have $^{232}\text{Th}/^{238}\text{U}$ ratios lower than 0.2, whereas the pre-2400 Ma analyses have a much wider spread of ratios.

6.2.5. T01-40 – Mafic Eclogite

A weighted mean of 28 analyses yielded a $^{207}\text{Pb}/^{206}\text{Pb}$ age of 1986 ± 29 Ma (2σ error, $\text{MSWD} = 0.69$) (Fig. 9e). Many of the analysed zircons were extremely low in uranium and thorium, but when only those analyses with $\text{Th}+\text{U} > 50$ ppm are averaged the weighted mean does not change significantly ($1972\pm 38/-39$ Ma, $\text{MSWD} = 0.12$). The $^{232}\text{Th}/^{238}\text{U}$ ratios of all the analyses range from 0.2-1.6 and a positive correlation is seen between $^{232}\text{Th}/^{238}\text{U}$ ratio and total $\text{Th}+\text{U}$ (Fig. 8 and Table 1) suggesting that Th is preferentially concentrated in grains with high total radiogenic element concentrations.

7. Discussion

7.1. Zircon Genesis and Significance of U-Pb Ages

Depletion in Th, with a coupled decrease in $^{232}\text{Th}/^{238}\text{U}$ ratio, is a feature that has been commonly reported in zircon rims that have undergone post-crystallisation isotope remobilisation [32-34, 37-42]. This is likely to be a function of the greater incompatibility of the larger Th ion in the zircon structure relative to that of U, and therefore preferential expulsion of Th during metamorphism or recrystallisation [33, 37, 39]. Observations of oscillatory luminescence zones passing from cores to rims (Fig. 4c,e,f), the presence of oscillatory zones in cores that are parallel to the grain boundaries (Figs. 4e,f and 6c), and core/rim boundaries that transgress the oscillatory zoning (Figs. 4c, e, f and 6c) when coupled with the Th depletion suggests that the Palaeoproterozoic rims in samples T01-05 and T01-19 did not form as new zircon overgrowths, but formed from pre-existing zircon, probably by the process of isostructural recrystallisation [e.g. 33].

Samples T01-05 (kyanite-garnet gneiss) and, to a lesser extent, T01-19 (blastomylonitic felsic gneiss), preserve rim compositions with intermediate Th and U concentrations

between two end members (Fig. 8), which suggests that Th was incompletely expelled from the zircon lattice during metamorphism. A significant gap exists in the $^{207}\text{Pb}/^{206}\text{Pb}$ age versus $^{232}\text{Th}/^{238}\text{U}$ plot (Fig. 8), which suggests that Pb was more thoroughly expelled than Th. Thus, the $^{207}\text{Pb}/^{206}\text{Pb}$ age is reset, but an elemental marker of the previous history of the grain remains. The distinct age gap between the cores and rims suggests core regions were not affected by Pb or Th loss, thus increasing confidence that the core ages truly represent the time of core formation.

Zircons from T01-12a (pegmatite) show a decrease in $^{232}\text{Th}/^{238}\text{U}$ ratio from core to rim that, unlike sample T01-05 and T01-19, results from increased values of both U and Th in the rims (Fig. 8). These rims have a euhedral prismatic habit and have near concordant ages with no observable spread outside analytical error (Fig. 9c). We interpret these rims to reflect zircon crystallisation by nucleation on xenocryst cores within a melt.

The mafic eclogite (T01-40) contains zircons with U and Th compositions that range over two orders of magnitude. A U versus Th plot reveals two distinct populations; analyses richer in both Th and U have higher $^{232}\text{Th}/^{238}\text{U}$ ratios (~ 1), whilst the less radiogenic grains have $^{232}\text{Th}/^{238}\text{U}$ ratios < 1 (Fig. 8). The identical formation ages of the light and dark zircon, universal anhedral form and multi-domain CL patterns suggest that both zircon textural groups formed during metamorphism. The low luminescent zircon is preferentially lower in Th, U and $^{232}\text{Th}/^{238}\text{U}$ ratio. Texturally this darker, low luminescent zircon occurs as rims and appears to invade pre-existing highly luminescent zircon (Fig. 7) suggesting an evolution of the metamorphic fluid co-existing with the zircon to higher levels of U and especially Th with time.

7.2. Implications for the Evolution of the Usagaran Orogen

7.2.1. Protolith age and provenance

Concordant zircon core $^{207}\text{Pb}/^{206}\text{Pb}$ ages range from 2427 ± 15 Ma to 3022 ± 10 Ma, with one younger grain at 2099 ± 31 Ma (1σ error)(Fig. 10a-d). The majority of grains form a broad peak between ~ 2740 to 2520 Ma with a prominent maxima at ~ 2720 Ma, which coincides with the age of the Tanzanian craton and with the protoliths of orthogneisses previously dated from the Isimani Suite [22](Fig. 10e), and a marked minima at ~ 2640 Ma (Fig. 10g).

The pelitic kyanite-garnet gneiss (T01-05) contains detrital zircons sourced from the Tanzanian craton and an as yet unknown 2400-2640 Ma source region. The protoliths of the two highly deformed felsic gneisses (T01-02 and T01-19) are less certain. They both contain a similar range of zircon core ages as the kyanite-garnet gneiss, suggesting that they consist, at least in part, of metasedimentary material derived from a similar source as T01-05. Their highly sheared nature and overall felsic composition means that tectonic mixing with some ~ 2700 Ma igneous material, similar to granite gneiss components of the Isimani Suite described by Reddy et al. [22], cannot be ruled out.

The source of the 2400-2640 Ma zircons is unknown and may represent an, as yet undated, component of the Tanzanian craton. However, the U-Pb age spectra of detrital zircons from the Itremo Group of central Madagascar indicates that central Madagascar (the Antananarivo Block and the unconformably overlying Itremo Group) was adjacent to East Africa at the time of deposition of the Itremo Group, which is constrained to between 1760 Ma and 800 Ma [43-45]. Central Madagascar and its northern continuation [17] was recently named Azania after the Greek name for the East African coast [46].

This region contains many rocks with protolith ages between 2.4 and 2.6 Ga [47-50] and would be a possible source of the zircons contained in the samples analysed here.

7.2.2. Timing of metamorphism and exhumation

In this study we have dated metamorphic zircons from the mafic eclogite that yield a weighted mean $^{207}\text{Pb}/^{206}\text{Pb}$ age of 1986 ± 29 Ma (2σ). Zircon rims that were isotopically reset during high grade metamorphism were dated from two samples: 1) a kyanite-garnet gneiss yielded a $^{207}\text{Pb}/^{206}\text{Pb}$ age of 1989 ± 10 Ma (2σ); 2) a blastomylonitic felsic gneiss yielded a $^{207}\text{Pb}/^{206}\text{Pb}$ age of $1997.6 \pm 2/-2.2$ Ma (2σ). These ages are all within error of each other and within error of a published U-Pb monazite dissolution age of 1999.5 ± 1.4 Ma from a pelite from the same area [3]. The coincidence of ages throughout the region suggests that eclogite-facies metamorphism affected all the main rock units in the study area and occurred at 1999.1 ± 1.1 Ma (2σ , MSWD = 0.99), which is a weighted mean of the complete U-Pb data from the four separate estimates of high-grade metamorphism.

Exhumation of the orogen is constrained by: 1) a U-Pb titanite age of 1996 ± 2 Ma [3]; 2) the intrusion age of the syn-post D_3 pegmatite (T01-12a) – 1991 ± 2 Ma – that cuts amphibolite-facies mylonitic deformation and is therefore younger than the amphibolite-facies retrogressive overprint, and; 3) the depositional age of the unconformably overlying Konse Group, dated by correlation of the Konse Group with the 1895 ± 27 Ma Ndembera volcanics [age recalculated from 25, using the decay constant of , 26].

The U-Pb zircon and published monazite data indicate the time of metamorphic crystallisation/recrystallisation because the maximum temperatures experienced by the rocks ($\sim 750^\circ\text{C}$) [3] is considerably lower than the closure temperature of Pb diffusion in

both zircon ($>1000^{\circ}\text{C}$) [51, 52] and monazite ($>900^{\circ}\text{C}$) [52]. It is hard to link the calculated ages directly with precise metamorphic conditions as the reactions responsible for monazite formation and zircon recrystallisation are not known in these rocks. However, Hoskin and Black [33] suggested that metamorphic zircon recrystallisation was thermoactivated and reduced lattice strain by the expulsion of large-radius trace elements. The resulting reduction in free energy restricts this process to prograde, near peak-temperature, metamorphic environments. Zircon rims in samples T01-05 and T01-19 are interpreted to have formed by solid-state zircon recrystallisation and therefore their age dates near near-peak temperature conditions. The published isothermal decompression curve [3, 5] indicates that peak temperatures may not have been reached at peak pressures, therefore the zircon age either dates eclogite-facies metamorphism, or the high temperature part of the decompression curve (Fig. 11).

Titanite has a closure temperature for Pb of $\sim 650^{\circ}\text{C}$ [53], therefore the U-Pb titanite data [3] dates the time the rock cooled below 650°C and constrains the higher temperature part of isothermal P-T curve [3] (Fig. 11). The difference between the U-Pb zircon and monazite ages and the U-Pb titanite age implies that the Isimani Suite cooled $\sim 150^{\circ}\text{C}$ in <6 Ma (Fig. 11). Pressures are harder to constrain as isotopic diffusion is a temperature-controlled process. However, a conservative pressure/time estimate based on the isothermal retrogression curve of Möller et al. [3] and Herms [5] is that in the 6 Ma the rocks must also have been exhumed a minimum of 0.4 GPa (~ 14 km) and a maximum of 1.3 GPa (~ 47 km)(Fig. 11). These cooling ($25^{\circ}\text{C}/\text{Ma}$) and exhumation rates (0.06-0.22 GPa/Ma) are comparable with those derived from Phanerozoic eclogite terranes [e.g. 10, 54].

Further constraints on the exhumation curve are provided by the 1991 ± 2 Ma age obtained from the syn-post D_3 pegmatite dyke. This post-dates the pervasive D_2 amphibolite-facies deformation that formed a sinistral transpressional zone [22] and was active during exhumation. Finally, the Konse Group is reported to unconformably overlie the Isimani Suite [19](Fig. 2b). This has been interpreted to be equivalent to the 1895 ± 27 Ma Ndembera volcanics [19, 20], suggesting exposure of the Isimani Suite by this time.

8. Conclusions

The timing of high-grade metamorphism and exhumation in the oldest known in-situ eclogite-facies terrane on Earth has been constrained by coupling U-Pb SIMS dating with CL imaging and trace element analysis. Our main conclusions are:

1. The eclogite-bearing Isimani Suite of the Usagaran Orogen was metamorphosed to eclogite-facies conditions ($\sim 750^\circ\text{C}$ and 1.8 GPa) [3] at, or immediately prior to 1999.1 ± 1.1 Ma.
2. Extensive sinistral transpressive deformation at amphibolite-facies conditions [22] is sealed by a syn-post D_3 pegmatite dated at 1991 ± 2 Ma.
3. Rapid exhumation rates of the eclogite-facies rocks are constrained to $\sim 25^\circ\text{C}/\text{Ma}$ and 0.06-0.22 GPa/Ma, consistent with exhumation rates of Phanerozoic eclogite and blueschist terranes.
4. Multiple origins for zircon rims have been interpreted from CL images. U and Th abundances and U-Pb ages. Zircon rims in pelitic and felsic metamorphic rocks preserve evidence of solid-state isostuctural recrystallisation that has partially, to

fully, reset the U-Pb isotopic systematics. New zircon overgrowths on xenocrysts in the pegmatite formed by crystallisation of new zircon from a melt.

5. Detrital zircon cores were dominantly derived from the Tanzanian craton and a second 2400-2640 Ma source region that is compatible with a belt of reworked Archaean and Palaeoproterozoic rocks that lies eastward in the East African Orogen [17].

Acknowledgements

This research was supported by the Australian Research Council by Small and Large Discovery grants to SMR and ASC. Fieldwork in Tanzania was facilitated by a number of people, but we especially thank Rev. Fr. Camillus Fillo Mitti of Rudi parish for his generous hospitality. The zircon analyses were carried out on the Sensitive High-mass Resolution Ion Microprobe mass spectrometer (SHRIMP II) operated by a consortium consisting of Curtin University of Technology, the Geological Survey of Western Australia, and the University of Western Australia with the support of the Australian Research Council. We appreciate the assistance of Peter Kinny, Sasha Nemchin and Allen Kennedy during SHRIMP analysis and data reduction. Ken Ludwig is thanked for providing copies of his programmes “Squid” and Isoplot” that were invaluable for data reduction and presentation. Paul Hoskin and Bradley Hacker are thanked for constructive and useful reviews and we wish to thank Ken Farley for editorial assistance. This contribution is TSRC publication #262.

References

- 1 P.J. O'Brien and J. Rötzler, High pressure granulites: formation, recovery of peak conditions and implications for tectonics, *Journal of Metamorphic Geology* 21, 3-20, 2003.
- 2 G. Zhao, P.A. Cawood, S.A. Wilde and L. Lu, High-pressure granulites (retrograded eclogites) from the Hengshan Complex, North China Craton: petrology and tectonic implications, *Journal of Petrology* 42, 1141-1170, 2001.
- 3 A. Möller, P. Appel, K. Mezger and V. Schenk, Evidence for a 2 Ga subduction zone: eclogites in the Usagarian belt of Tanzania, *Geology* 23, 1067-1070, 1995.
- 4 E.V. Sklyarov, D.P. Gladkochub, A. Mruma, K. Theunissen, A.I. Melnikov and J. Klerkx, Paleoproterozoic eclogites and garnet pyroxenites of the Ubende Belt (Tanzania), *Schweizerische Mineralogische und Petrographische Mitteilungen* 78(2), 257-271, 1998.
- 5 P. Herms, Fluids in a 2 Ga old subduction zone - deduced from eclogite-facies rocks of the Usagaran belt, Tanzania, *European Journal of Mineralogy* 14, 361-373, 2002.
- 6 P. Tuisku and H. Huhma, Eclogite from the SW-marginal zone of the Lapland Granulite belt: evidence from the 1.90-1.88 Ga subduction zone, in: *International Ophiolite Symposium and Field Excursion: Generation and Emplacement of Ophiolites Through Time*, E. Hanski and J. Vuollo, eds., pp. 61, Geological Survey of Finland, Oulu, Finland, 1998.
- 7 A.P. Smelov and V.I. Beryozkin, Retrograded eclogites in the Olekma granite-greenstone region, Aldan Shield, *Precambrian Research* 62, 419-430, 1993.

- 8 J.A. Baldwin, S.A. Bowring and M.L. Williams, Petrological and geochronological constraints on high pressure, high temperature metamorphism in the Snowbird tectonic zone, Canada, *Journal of Metamorphic Geology* 21, 81-98, 2003.
- 9 B.R. Hacker, L. Ratschbacher, L. Webb, M.O. McWilliams, T. Ireland, A. Calvert, S. Dong, H.-R. Wenk and D. Chateigner, Exhumation of ultrahigh-pressure continental crust in east central China: Late Triassic-Early Jurassic tectonic unroofing., *Journal of Geophysical Research* 105(B6), 13339-13364, 2000.
- 10 S.M. Reddy, J. Wheeler and R.A. Cliff, The geometry and timing of orogenic extension: an example from the Western Italian Alps, *Journal of Metamorphic Geology* 17, 573-589, 1999.
- 11 D.A. Carswell, *Eclogite-facies rocks*, Blackie, 1990.
- 12 R.C. Newton, Metamorphic temperatures and pressures of Group B and C eclogites, in: *Blueschists and Eclogites*, B.W. Evans and E. Brown, eds., Geological Society of America Memoir 164, 1986.
- 13 S. Muhongo, A. Kröner and A.A. Nemchin, Single zircon evaporation and SHRIMP ages for granulite-facies rocks in the Mozambique belt of Tanzania, *Journal of Geology* 109, 171-189, 2001.
- 14 A. Möller, K. Mezger and V. Schenk, U-Pb dating of metamorphic minerals: Pan-African metamorphism and prolonged slow cooling of high pressure granulites in Tanzania, East Africa, *Precambrian Research* 104, 123-146, 2000.

- 15 R.J. Stern, Arc Assembly and continental collision in the Neoproterozoic East African orogeny - implications for the consolidation of Gondwana, *Annual Review of Earth and Planetary Sciences* 22, 319-351, 1994.
- 16 I.W.D. Dalziel, Neoproterozoic-Paleozoic geography and tectonics: Review, hypothesis, environmental speculation, *Geological Society of America Bulletin* 109, 16-42, 1997.
- 17 A.S. Collins and B.F. Windley, The Tectonic Evolution of central and northern Madagascar and its place in the Final Assembly of Gondwana, *Journal of Geology* 110, 325-340, 2002.
- 18 K.D. Meinhold, Petrographie, Metamorphose, Tektonik und stratigraphische Stellung der Konse-Serie in Zentral-Tanzania (Ostafrika), Beihefte zum *Geologischen Jahrbuch* 91, 1-137, 1970.
- 19 A.H. Mruma, Stratigraphy, Metamorphism and Tectonic evolution of the Early Proterozoic Usagaran belt, Tanzania, University of Oulu, Finland, 1989.
- 20 J.K. Whittingham, *The Geology of the Nyanzwa Area*, 27 pp., 1959.
- 21 J.R. Harpum, Summary of the Geology of Tanzania, Part V: Structure and Geotectonics of the Precambrian, 58 pp., Mineral Resources Division, Government of Tanzania, Dodoma, 1970.
- 22 S.M. Reddy, A.S. Collins and A. Mruma, Complex High-Strain Deformation in the Usagaran Orogen, Tanzania: Structural Setting of Palaeoproterozoic Eclogites, *Tectonophysics* 375, 101-123, 2003.

- 23 A. Möller, K. Mezger and V. Schenk, Crustal age domains and the evolution of the continental crust in the Mozambique belt of Tanzania: combined Sm-Nd, Rb-Sr, and Pb-Pb isotopic evidence, *Journal of Petrology* 39, 749-783, 1998.
- 24 M.A.H. Maboko and E. Nakamura, Nd and Sr isotopic mapping of the Archaean-Proterozoic boundary in southeastern Tanzania using granites as probes for crustal growth, *Precambrian Research* 77, 105-115, 1996.
- 25 I. Wendt, C. Besang, W. Harre, H. Kreuzer, H. Lenz and P. Müller, Age determinations of granitic intrusions and metamorphic events in the early Precambrian of Tanzania, 24th International Geological Congress, Montreal - section 1, 295-314, 1972.
- 26 R.H. Steiger and E. Jager, Subcommittee on geochronology: convention on the use of decay constants in geo- and cosmo-chronology, *Earth and Planetary Science Letters* 36, 359-362, 1977.
- 27 G. Gabert and I. Wendt, Datierung von granitischen Gesteinen im Dodoman- und Usagaran-System und in der Ndembera-Serie (Tanzania), *Geologisches Jahrbuch* B11, 3-55, 1974.
- 28 S.M. Reddy, A.S. Collins, C. Buchan and A. Mruma, Preliminary $^{40}\text{Ar}/^{39}\text{Ar}$ data from the Usagaran Orogen, Tanzania: A reassessment of Neoproterozoic reworking of Palaeoproterozoic tectonism, *Journal of African Earth Sciences*, in press.
- 29 W. Compston, I.S. Williams and C. Meyer, U-Pb geochronology of zircons from lunar breccia 73217 using a sensitive high mass-resolution ion microprobe, *Journal of Geophysical Research* 89(Supplement), B525-B534, 1984.

- 30 J.R. Hinthorne, C.A. Anderson, R.L. Conrad and J.F. Lovering, Single-grain $^{207}\text{Pb}/^{206}\text{Pb}$ and U/Pb age determinations with a 10 μm spatial resolution using the ion microprobe mass analyser (IMMA), *Chemical Geology* 25, 271-303, 1979.
- 31 D.R. Nelson, Compilation of SHRIMP U-Pb zircon geochronology data, 1996, Geological Survey of Western Australia, Perth, Australia, 1997.
- 32 R.T. Pidgeon, A.A. Nemchin and G.J. Hitchen, Internal structures of zircons from Archaean granites from the Darling Range batholith: implications for zircon stability and the interpretation of zircon U-Pb ages, *Contributions to Mineralogy and Petrology* 132, 288-299, 1998.
- 33 P.W.O. Hoskin and L.P. Black, Metamorphic zircon formation by solid-state recrystallisation of protolith igneous grains, *Journal of Metamorphic Geology* 18, 423-439, 2000.
- 34 G. Vavra, R. Schmid and D. Gebauer, Internal morphology, habit and U-Th-Pb microanalysis of amphibolite-to-granulite facies zircons: geochronology of the Ivrea Zone (Southern Alps), *Contributions to Mineralogy and Petrology* 134, 380-404, 1999.
- 35 F. Corfu, J.M. Hanchar, P.W.O. Hoskin and P.D. Kinny, Atlas of zircon textures, in: *Zircon*, J.M. Hanchar and P.W.O. Hoskin, eds. 53, pp. 468-500, Mineralogical Society of America, Reviews in Mineralogy and Geochemistry, Washington, D.C., 2003.

- 36 D. Gebauer, H.P. Schertl, M. Brix and W. Schreyer, 35 Ma old ultrahigh-pressure metamorphism and evidence for very rapid exhumation in the Dora Maira Massif, Western Alps, *Lithos* 41, 5-24, 1997.
- 37 R.T. Pidgeon, Recrystallisation of oscillatory-zoned zircon: some geochemical and petrological implications, *Contributions to Mineralogy and Petrology* 110, 463-472, 1992.
- 38 A.S. Collins, Structure and Age of the Northern Leeuwin Complex, Western Australia: Constraints from Field Mapping and U-Pb Isotopic Analysis, *Australian Journal of Earth Sciences* 50, 585-599, 2003.
- 39 R. Maas, P.D. Kinny, I.S. Williams, D.O. Froude and W. Compston, The Earth's oldest known crust: A geochronological and geochemical study of 3900-4200 Ma old detrital zircons from Mt. Narryer and Jack hills, Western Australia, *Geochimica et Cosmochimica Acta* 56, 1281-1300, 1992.
- 40 D. Rubatto, D. Gebauer and R. Compagnoni, dating of eclogite-facies zircons: the age of Alpine metamorphism in the Sesia-Lanzo Zone (Western Alps), *Earth & Planetary Science Letters* 167, 141-158, 1999.
- 41 I.S. Williams, I.S. Buick and I. Cartwright, An extended episode of early Mesoproterozoic metamorphic fluid flow in the Reynolds Range, central Australia, *Journal of Metamorphic Geology* 14, 29-47, 1996.
- 42 L.D. Ashwal, R.D. Tucker and E.K. Zinner, Slow cooling of deep crustal granulites and Pb-loss in zircon, *Geochimica et Cosmochimica Acta* 63, 2839-2851, 1999.

- 43 R. Cox, D.S. Coleman, C.B. Chokel, S.B. DeOreo, A.S. Collins, A. Kröner and B. De Waele, Proterozoic tectonostratigraphy and paleogeography of central Madagascar derived from detrital zircon U-Pb age populations, *Journal of Geology*, in press.
- 44 A.S. Collins, A. Kröner, I.C.W. Fitzsimons and T. Razakamanana, Detrital Footprint of the Mozambique Ocean: U/Pb SHRIMP and Pb Evaporation Zircon Geochronology of Metasedimentary Gneisses in Eastern Madagascar, *Tectonophysics* 375, 77-99, 2003.
- 45 A.S. Collins, S. Johnson, I.C.W. Fitzsimons, C.M. Powell, B. Hulscher, J. Abello and T. Razakamanana, Neoproterozoic deformation in central Madagascar: a structural section through part of the East African Orogen, in: *Proterozoic East Gondwana: Supercontinent Assembly and Breakup*, M. Yoshida, B. Windley and S. Dasgupta, eds. 206, pp. 363-379, Special Publication of the Geological Society, London, 2003.
- 46 A.S. Collins, S.A. Pisarevsky, P.D. Kinny, M. Santosh and I.C.W. Fitzsimons, Late Neoproterozoic/Cambrian Palaeogeography of the central East African Orogen, in: *20th Colloquium of African Geology*, Orléans, France, in press.
- 47 J.-L. Paquette and A. Nédélec, A new insight into Pan-African tectonics in the East-West Gondwana collision zone by U-Pb zircon dating of granites from central Madagascar, *Earth and Planetary Science Letters* 155, 45-56, 1998.
- 48 R.D. Tucker, L.D. Ashwal, M.J. Handke, M.A. Hamilton, M. Le Grange and R.A. Rabeloson, U-Pb geochronology and isotope geochemistry of the Archean and

- Proterozoic rocks of north-central Madagascar, *Journal of Geology* 107, 135-153, 1999.
- 49 A. Kröner, E. Hegner, A.S. Collins, B.F. Windley, T.S. Brewer, T. Razakamanana and R.T. Pidgeon, Age and Magmatic History of the Antananarivo Block, Central Madagascar, as Derived from Zircon Geochronology and Nd Isotopic Systematics, *American Journal of Science* 300, 251-288, 2000.
- 50 A.S. Collins, I.C.W. Fitzsimons, P.D. Kinny, T.S. Brewer, B.F. Windley, A. Kröner and T. Razakamanana, The Archaean Rocks of Central Madagascar: Their Place in Gondwana., in: 4th International Archaean Symposium 2001, Extended Abstracts. AGSO - Geoscience Australia, Record 2001/37, K.F. Cassidy, J.M. Dunphy and M.J. Van Kranendonk, eds., pp. 294-296, 2001.
- 51 A. Möller, P.J. O'Brien, A. Kennedy and A. Kröner, Polyphase zircon in ultrahigh-temperature granulites (Rogaland, SW Norway): constraints for Pb diffusion in zircon, *Journal of Metamorphic Geology* 20, 727-740, 2002.
- 52 D.J. Cherniak and E.B. Watson, The influence of diffusion on U-Pb systematics, in: 11th Annual Goldschmidt Conference, pp. Abstract 3260, 2001.
- 53 D.J. Cherniak, Lead diffusion in titanite and preliminary results on the effects of radiation damage on Pb transport, *Chemical Geology* 110, 177-194, 1993.
- 54 R.P. Wintsch, T. Byrne and M. Toriumi, Exhumation of the Sanbagawa blueschist unit, SW Japan, by lateral flow and extrusion: evidence from structural kinematics and retrograde P-T-t paths, in: *Exhumation Processes: Normal Faulting, Ductile Flow and Erosion*, U. Ring, M.T. Brandon, G.S. Lister and S.D. Willett, eds., pp. 129-155, Geological Society, London, Special Publication 154, London, 1999.

- 55 J.H. Guo, P.J. O'Brien and M.G. Zhai, High pressure granulites in the Sangan area, North China Craton: metamorphic evolution, P-T paths and geotectonic significance, *Journal of Metamorphic Geology* 20, 741-757, 2002.
- 56 C.J. Wei, C.G. Zhang, A.L. Zhang, T.H. Wu and J.H. Li, Metamorphic P-T conditions and geological significance of high-pressure granulite from the Jianping complex, western Liaoning province, *Acta Petrologica Sinica* 17, 269-282, 2001.
- 57 S.W. Faryad, Metamorphic evolution of the Precambrian South Badakhshan block, based on mineral reactions in metapelites and metabasites associated with whiteschists from Sare Sang (Western Hindu Kush, Afghanistan), *Precambrian Research* 98, 223-241, 1999.
- 58 F.S. Spear, *Metamorphic Phase Equilibria and Pressure-Temperature-Time Paths*, 799 p. pp., Mineralogical Society of America, Washington D.C., 1993.
- 59 J.K. Whittingham, Geological map of Nyanzwa-south B37/S 1. Quarter degree sheet 198, Geological Survey Department, Dodoma, 1954.

Figure Captions

Figure 1: Pressure-temperature plot showing the published paths of the pre-1500 Ma moderate temperature and overprinted eclogite types of high pressure granulites [as defined by, and figure modified from, 1]. 1 = Usagaran Belt, Tanzania [3, 5]; 2 = Hengshan Belt, China [2]; 3 = Sanggan Belt, China [55]; 4 = Ubendian Belt, Tanzania [4]; 5 = Jianping Belt, China [56]; 6 = Sare Sang, Badakhshan Block, Afghanistan [57]; 7 = Snowbird tectonic zone, Canada [8]; * = Lapland Granulite Belt [6]. Thick arrows refer

to Usagaran/Ubende eclogites. Field for Phanerozoic subduction zone metamorphism and metamorphic facies (thick grey curves) after Spear [58]. High-pressure granulite field after O'Brien and Rötzler [1]. Aluminosilicate polymorph fields plotted for reference, And = andalusite, Ky = kyanite, Sill = sillimanite. Amph = Amphibolite.

Figure 2: a) Geological map of part of East Africa with cross ornamentation marking Archaean rocks, dark grey delineating Palaeoproterozoic rocks, light grey indicating Mesoproterozoic and Neoproterozoic rocks and the stippled ornamentation indicating Phanerozoic rocks, (b) indicates the location of Fig 2b. b) Geological map of part of the Usagaran Orogen, Tanzania. Map and lithological subdivisions are after Mruma [19] and Whittingham [59]. Asterisks mark the location of samples discussed in this paper; all samples are prefixed by "T01".

Figure 3: Field photographs of outcrops and samples discussed in the text. a) Kyanite-garnet gneiss (T01-05) with boudins of garnet amphibolite. b) 20-40 cm-thick pegmatite (T01-12a) cutting amphibolite-facies S2 mylonite fabric. The pegmatite intrudes parallel to an F_3 axial surface. c) δ -type inclusion of polycrystalline quartz in a blastomylonitic felsic gneiss (T01-19). d) Yalumba Hill from Rudi village (see Fig.2 for location) the location of T01-40 is marked.

Figure 4: CL images of characteristic zircon grains and SHRIMP analytical spots from sample T01-02 (a-b) and T01-05 (c-f). a) High-contrast CL image of Grain 12 displaying

an irregular, moderately luminescing partial rim that protrudes into the middle of the grain crosscutting poorly luminescent zones in the core of the grain. b) Grain 03, has a thick, brightly luminescent rim with broad luminescent bands and cracks that radiate from a dark core. c) Grain 04 from T01-05. Simple broad concentric banding in the core and sympathetic patchy oscillatory zoning in rim are overprinted by zones of highly heterogeneous textures that are concentrated at the core/rim boundary. This boundary broadly follows the grain margin. d) Grain 03, with a poorly luminescent oscillatory core and rim separated by a bright luminescent band. e) Grain 07 with parallel oscillatory zoning in the core and rim separated by highly heterogeneous luminescent zircon that defines an irregular core-rim boundary. f) Grain 08, with poorly luminescent oscillatory zoned zircon in the core passing sympathetically into brightly luminescent oscillatory zoned rim zircon through a roughly grain-margin parallel core-rim boundary that displays <10 μ m-scale protuberances into the core. In T01-05 zircon rims always have lower $^{232}\text{Th}/^{238}\text{U}$ ratios than those of the core.

Figure 5: Backscatter electron and CL images of characteristic zircon grains and SHRIMP analytical spots from pegmatite sample T01-12a. a) Backscatter electron image of a selection of grains demonstrating their euhedral morphology and pyramidal prism terminations. Cores are faintly visible as slightly darker regions within the crystals. Numbers refer to SHRIMP analysis sites: 2.1 – $^{207}\text{Pb}/^{206}\text{Pb}$ age = 2732 ± 27 Ma, $^{232}\text{Th}/^{238}\text{U}$ = 0.68, 2.2 - $^{207}\text{Pb}/^{206}\text{Pb}$ age = 1986 ± 6 Ma, $^{232}\text{Th}/^{238}\text{U}$ = 0.05, 6.1 – $^{207}\text{Pb}/^{206}\text{Pb}$ age = 2774 ± 9 Ma, $^{232}\text{Th}/^{238}\text{U}$ = 0.41, 6.2 – $^{207}\text{Pb}/^{206}\text{Pb}$ age = 1993 ± 4 Ma, $^{232}\text{Th}/^{238}\text{U}$ = 0.06. Details of crystals 10 and 11 are given in c) and d) respectively. b), c) and d) CL images

of individual zircon crystals demonstrating the euhedral habit and distinctly bright luminescent cores surrounded by thick poorly luminescent rims. The outline of the crystal in (b) is highlighted as the rim contrasts poorly with the mount. In (c) and (d) the cores have been separately imaged at a lower contrast to the rims to increase resolution.

Figure 6: CL images of characteristic zircon grains and SHRIMP analytical spots from blastomylonitic felsic gneiss sample T01-19. a) Grain 04, which displays a distinct core surrounded by zircon with broad poorly luminescent banding. b) Oscillatory zoned core and first rim (Rim 1) that are separated by the development of pyramidal faces in Rim 1 at the expense of the basal pinacoid in the core. A second then, poorly luminescent, rim (Rim 2) has developed around much of the grain and truncates the banding of Rim 1. Zone controlled patchy zircon overgrowths also occur within the oscillatory parts of the zircon. c) Grain 11, with an oscillatory zoned core separated from a poorly luminescent broadly zoned rim by a highly luminescent band (labelled “bright band”) that truncates the core oscillatory banding. d) High-contrast CL image of Grain 18, showing subtle oscillatory zoning within a poorly luminescent zircon. The zircon is partially rimmed with a very thin brightly luminescent rim.

Figure 7: CL images of characteristic zircon grains and SHRIMP analytical spots from mafic eclogite sample T01-40. a) Anhedral zircon (Grain 21) with brightly luminescent zircon apparently replaced by poorly luminescent zircon along individual planar oscillatory zones. b) Grain 06 with sector zoned brightly luminescent zircon rimmed by homogenous poorly luminescent zircon. c) Subhedral zircon (Grain 17) with faintly

luminescent concentric zones preserved in the core and a $\sim 10\mu\text{m}$ rim of poorly luminescent zircon. d) Anhedral crystal (Grain 10) with moderately luminescent zircon apparently transgressing a core of highly luminescent zircon. e) Grain 05, sector zoned highly luminescent core with two rims of less highly luminescent zircon. The inner rim has an irregular boundary with the core region. f) Grain 07, subhedral zircon with a sector zoned core and a poorly luminescent rim.

Figure 8: Plots of Th and U abundances, $^{232}\text{Th}/^{238}\text{U}$ ratios and $^{207}\text{Pb}/^{206}\text{Pb}$ ages. Errors are not shown for clarity, but are $\pm 20\%$ for U and Th abundances and commonly $< 1\%$ for $^{207}\text{Pb}/^{206}\text{Pb}$ ages, except in T01-40 where the low concentrations of U and Th is reflected in a considerable error in some analyses (see Table 1). Arrows indicate the interpreted trend in the data. Undif. = homogenous and undifferentiated grains. The key for T01-02, T01-05, T01-12a, T01-19 is located in the first diagram. T01-40 has a separate key that is located on the relevant diagram. Lines representing Th/U ratios of 1 and 0.1 are drawn on each U versus Th plot.

Figure 9: U-Pb concordia plots of SHRIMP data for samples T01-02 (a), T01-05 (b), T01-12a (c), T01-19 (d) and T01-40 (e). Error ellipses and single age analyses are quoted at the 1σ level, weighted means of multiple analyses and discordia intercepts are quoted at the 2σ level.

Figure 10: Probability distribution diagrams of zircon cores (as defined by CL textures) from samples T01-02, T01-05, T01-12a, T01-19. Note the uncertainty in the significance in the zircon ages from T01-02 discussed in the text. In addition, core analyses from T01-24 and T01-01, also from the Great Ruaha River traverse (location on Fig. 2) and presented in Reddy et al. [22], are presented for comparison. a-f – only core analyses that are >90% concordant are plotted and the grey line marks the interpreted crystallisation age of the protolith of the orthogneiss T01-24 and the age of voluminous granites in the Tanzanian craton. g) All data from this study, illustrating the broad peak between 2740 to 2520 Ma with a prominent maxima at ~2720 Ma and a minima at ~2640 Ma.

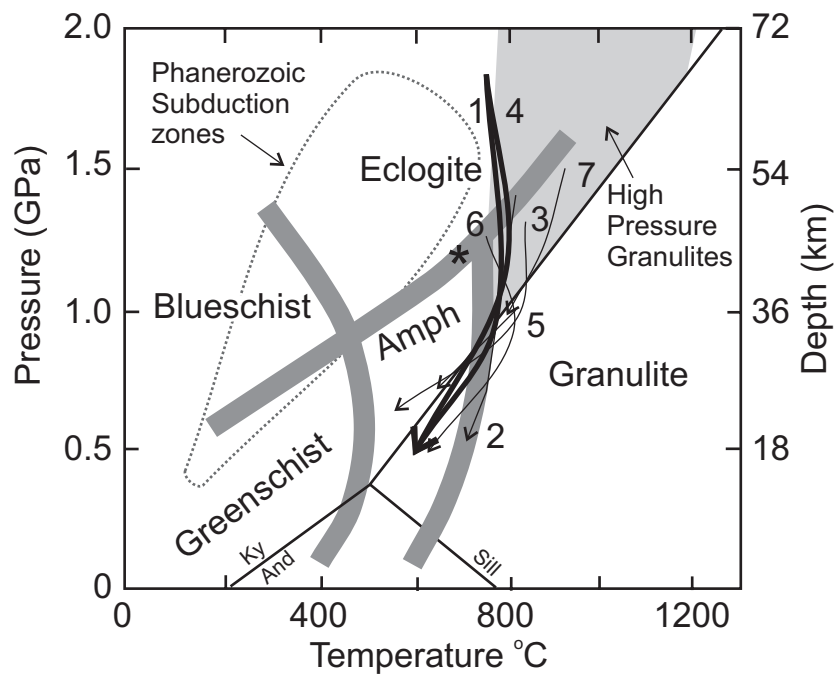
Figure 11: Summary pressure-temperature plot showing the published exhumation path of the Usagaran eclogite-facies rocks [3, 5] with time constraints determined in this study and by Möller et al. [3]. The retrogression path is here extended to colder, lower pressure regions by the work presented in this paper and the inference that the rocks were exhumed and unconformably overlain by the Konse Group that is dated at 1895 ± 27 Ma (by analogy with the Ndembera volcanics). Abbreviations as Fig 1 except – Gst = Greenschist.

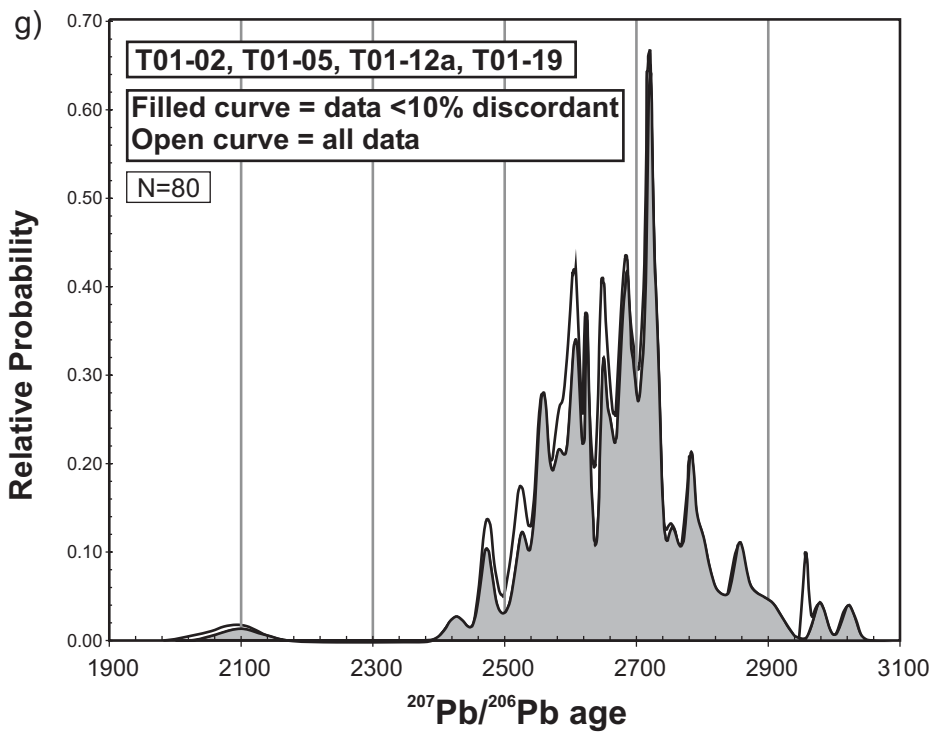
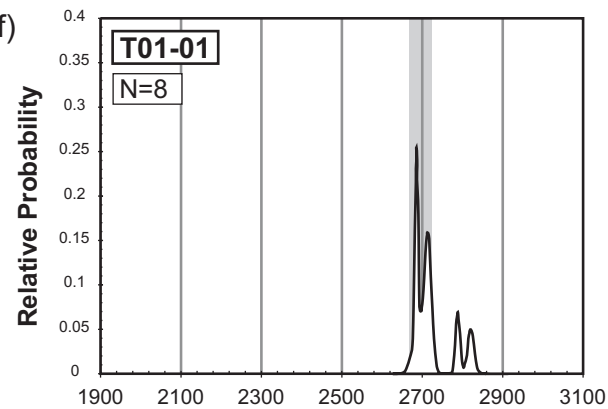
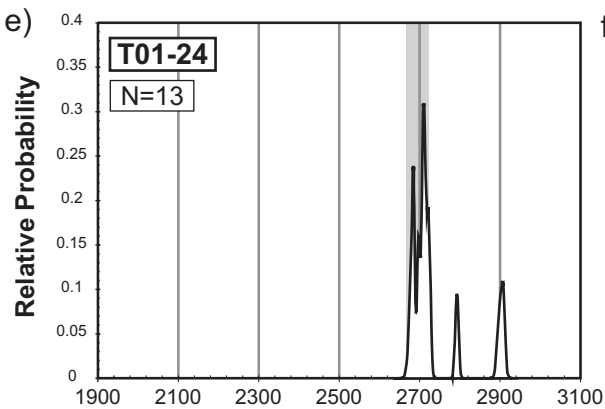
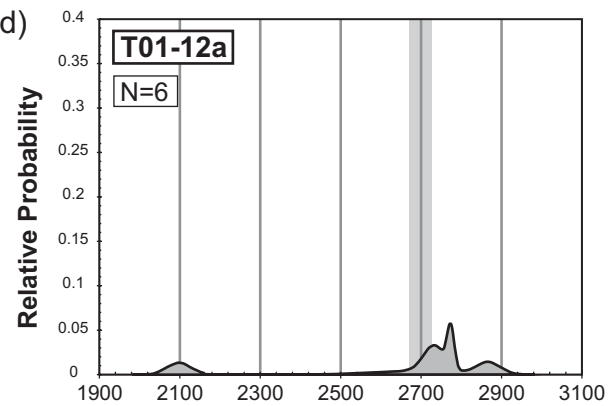
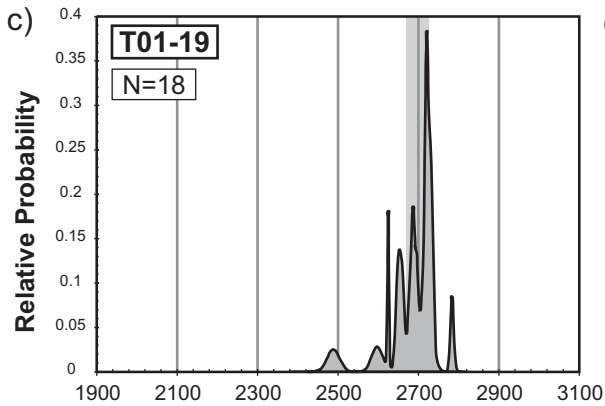
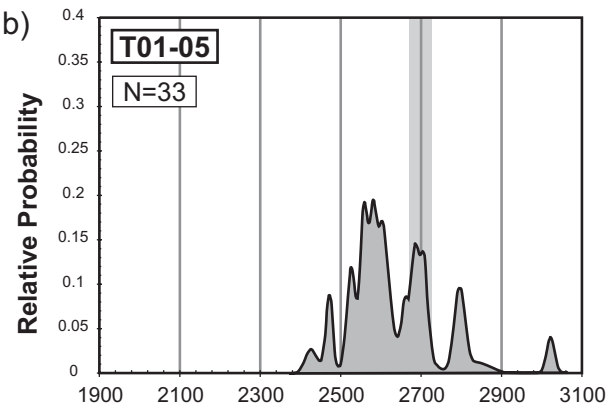
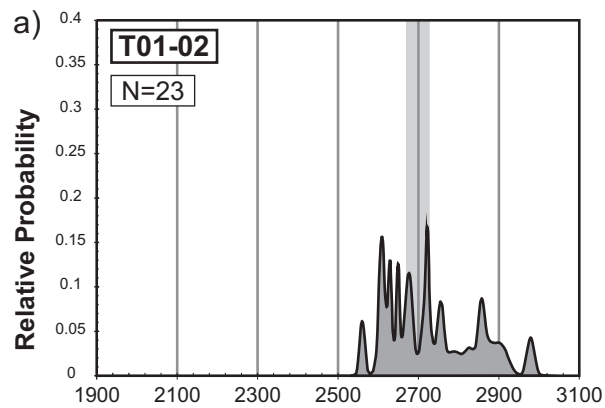
Table Captions

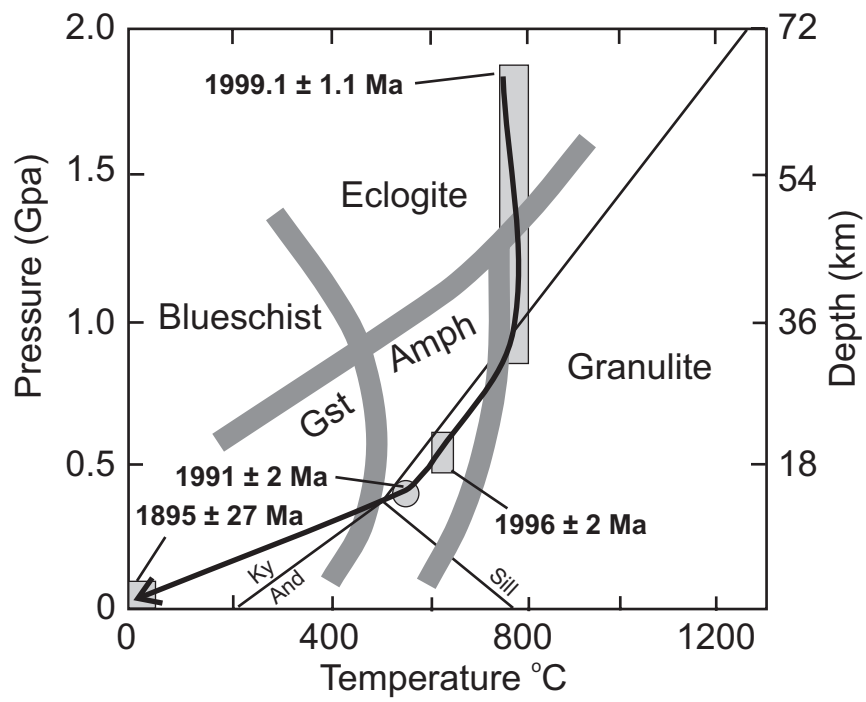
Table 1: U-Pb SHRIMP data. ‘%com. ^{206}Pb ’ is the percentage of non-radiogenic ^{206}Pb in the measured total, ‘% disconc’ is the percentage discordant. Ages are in Ma, with errors quoted at 1σ . ‘c’ represents core analyses, ‘r’ represents rim analyses, ‘hom’

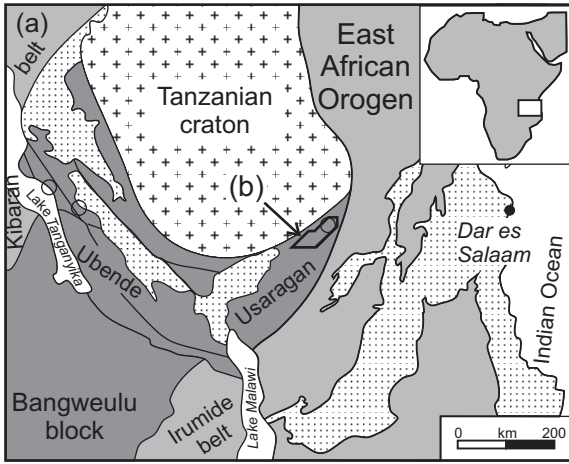
represents analyses from a homogenous grain. For Sample T01-40, “l” identifies an analysis on a highly luminescent zircon, “d” refers to an analysis on a poorly luminescent zircon.

Table 2: U-Pb SHRIMP standard data. Individual SHRIMP sessions are cross-referenced with the unknown data in Table 1.

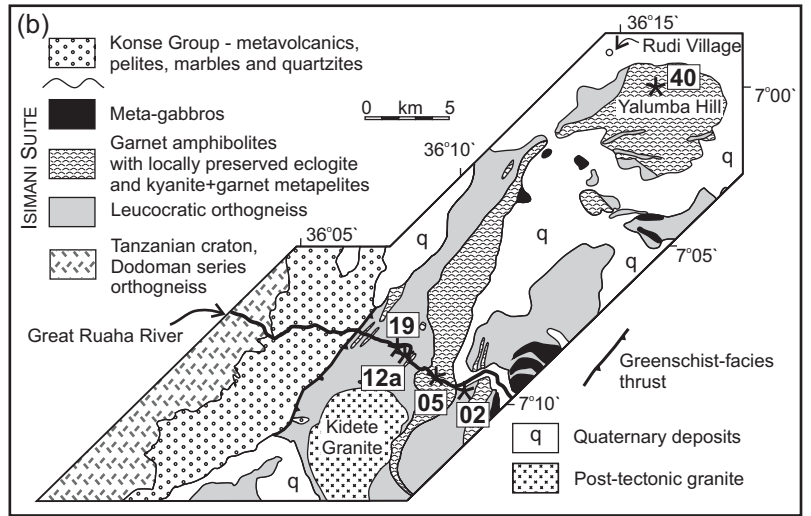


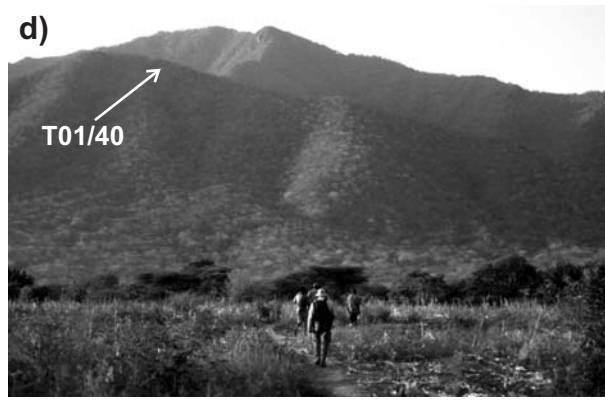
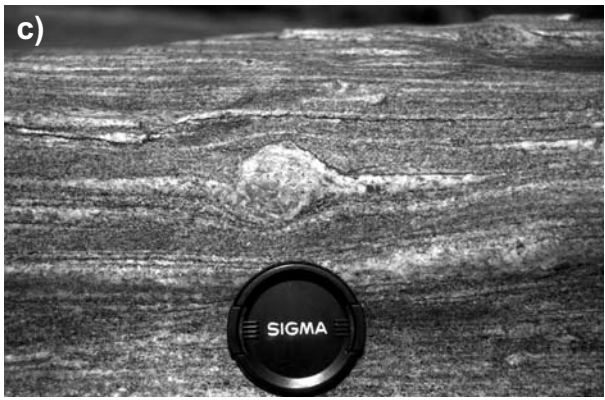
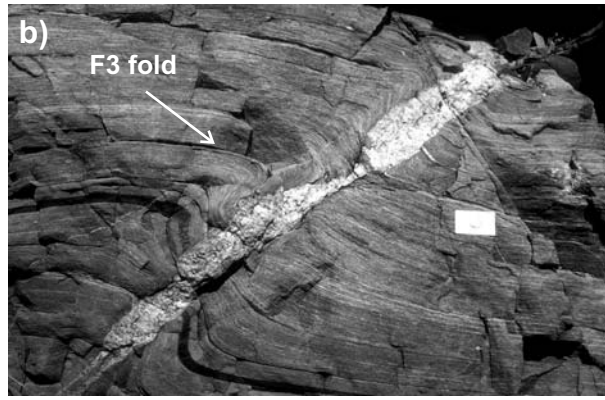
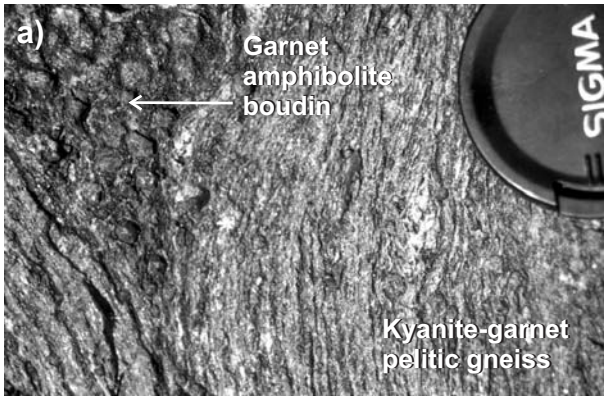


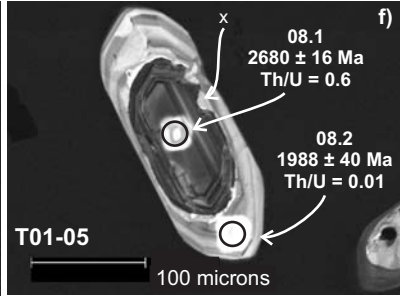
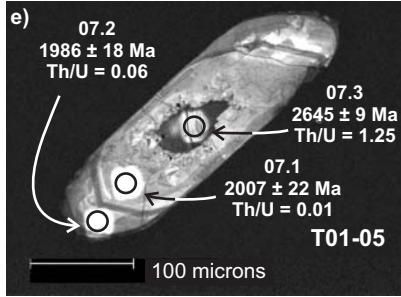
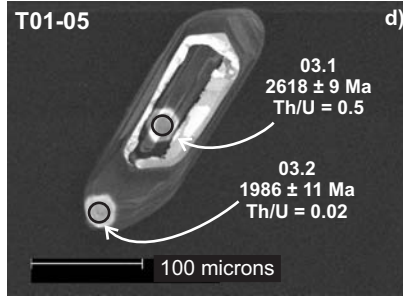
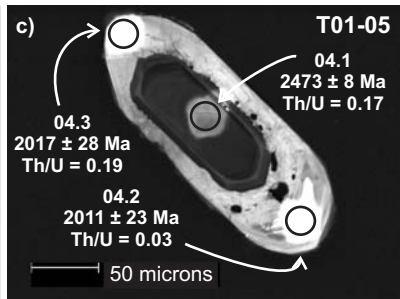
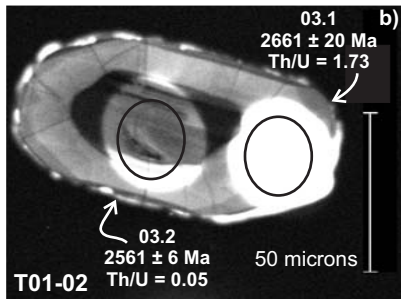
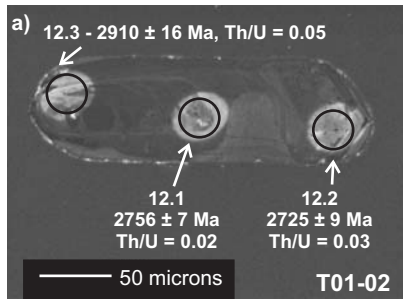


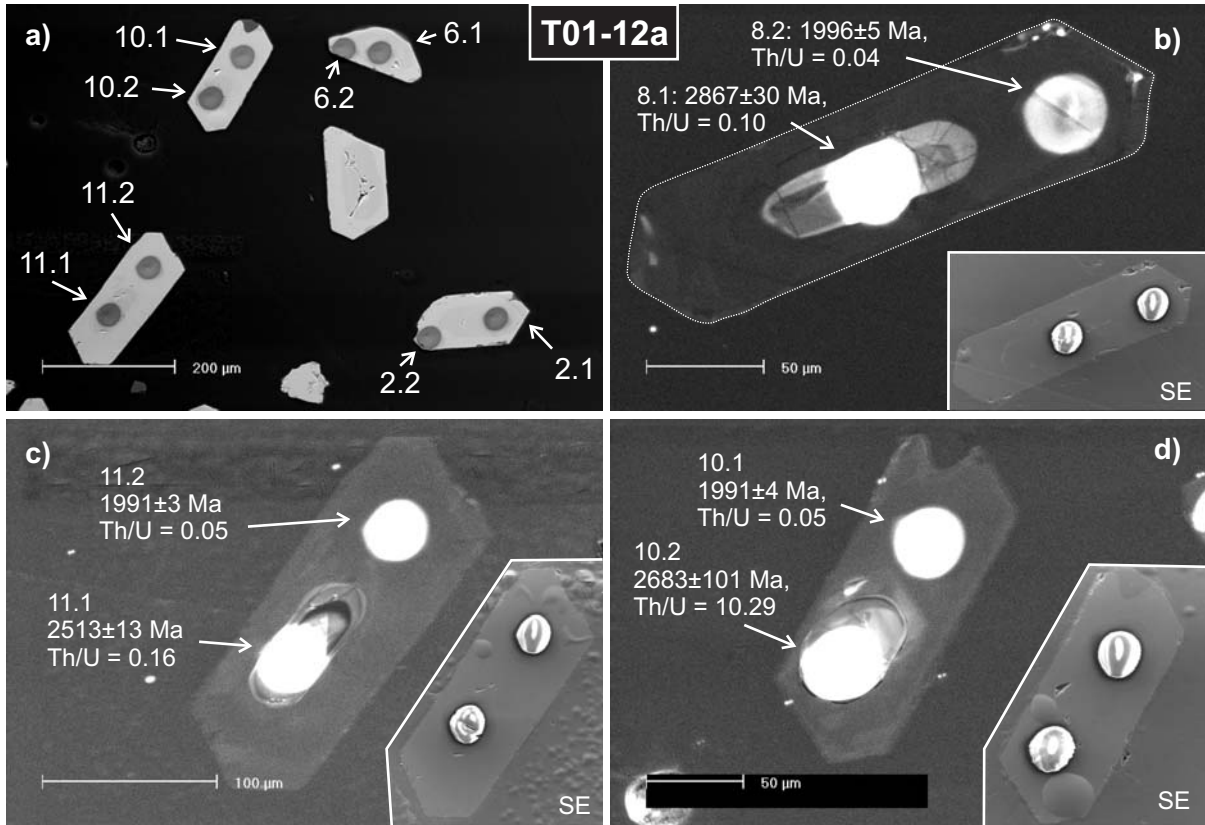


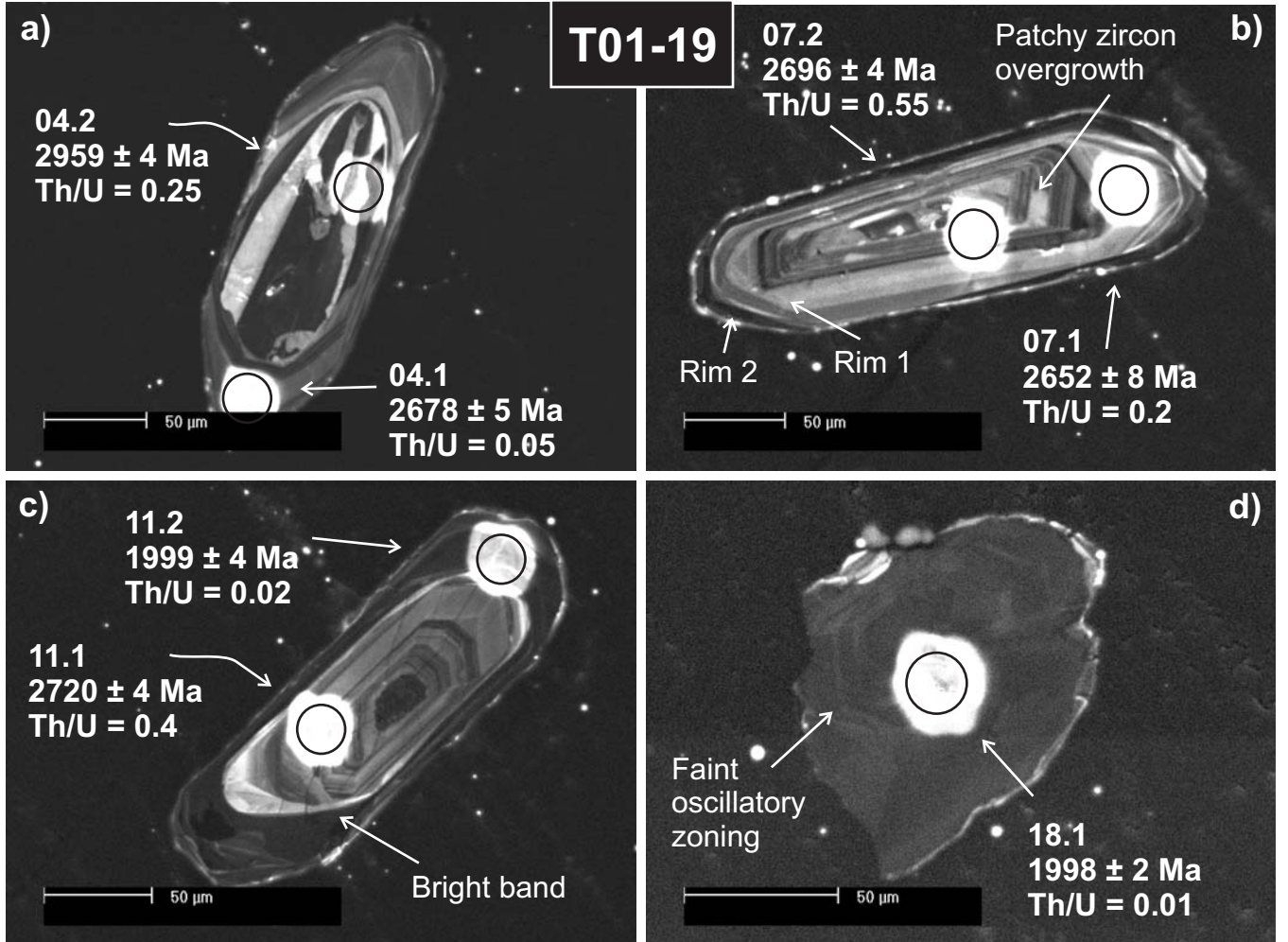
○ = Known location of eclogite-facies rocks after Moller et al. [3] and Sklyarov et al. [4]

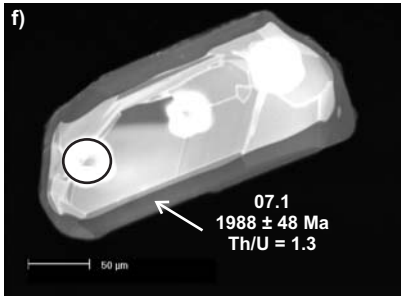
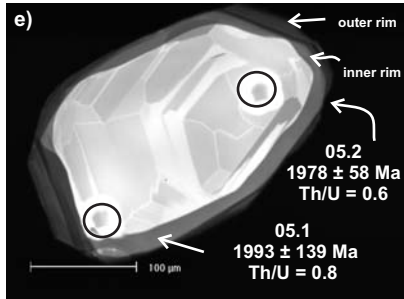
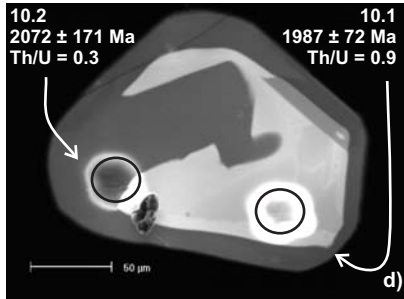
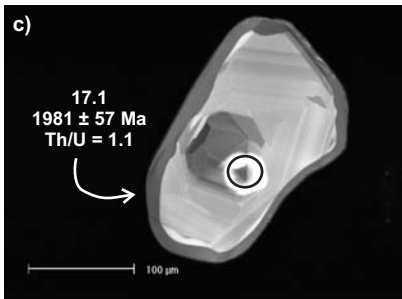
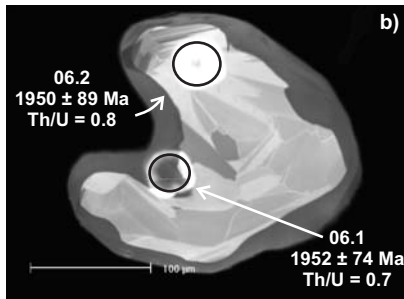
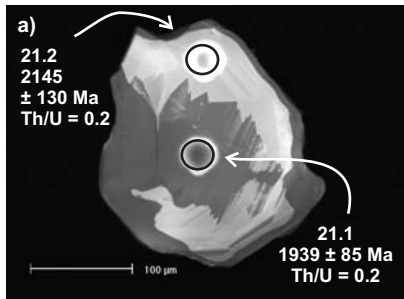


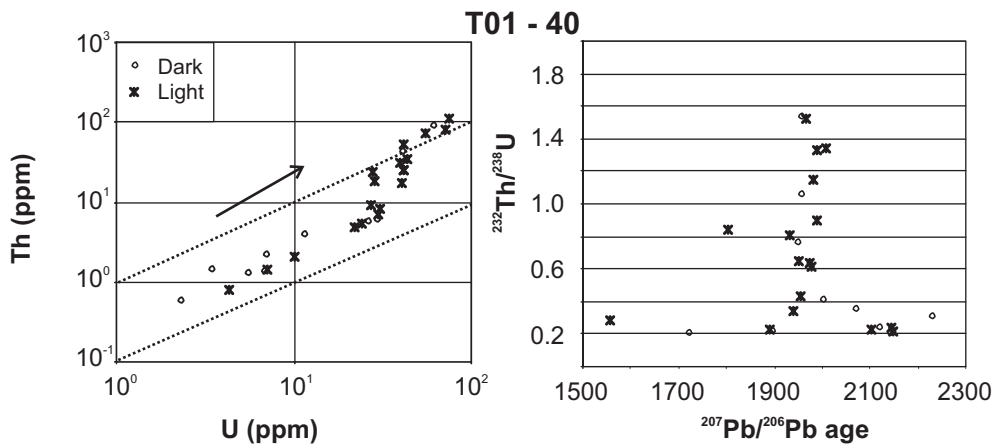
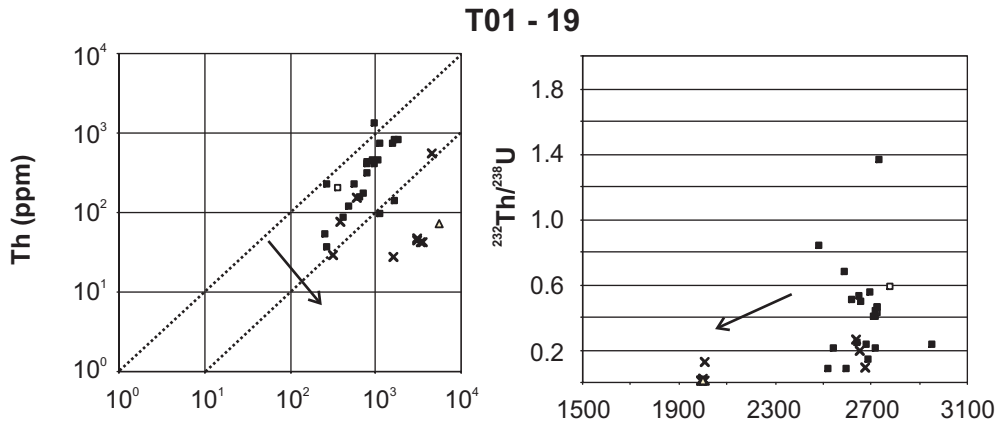
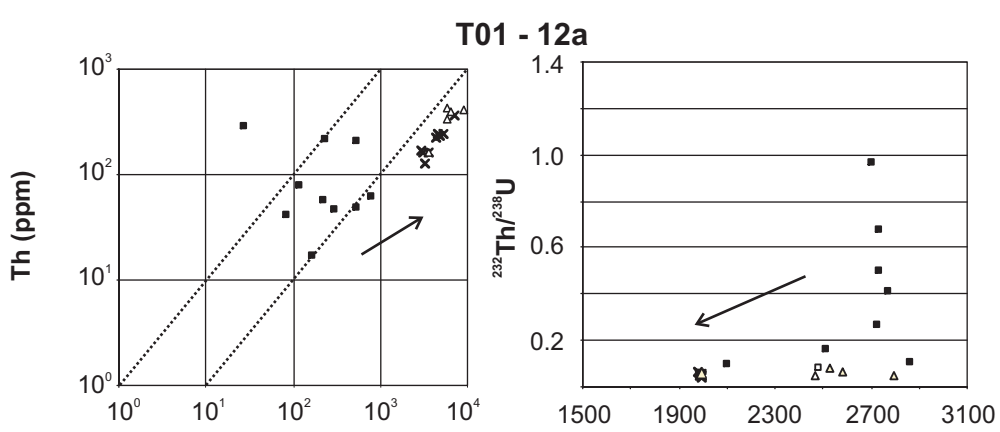
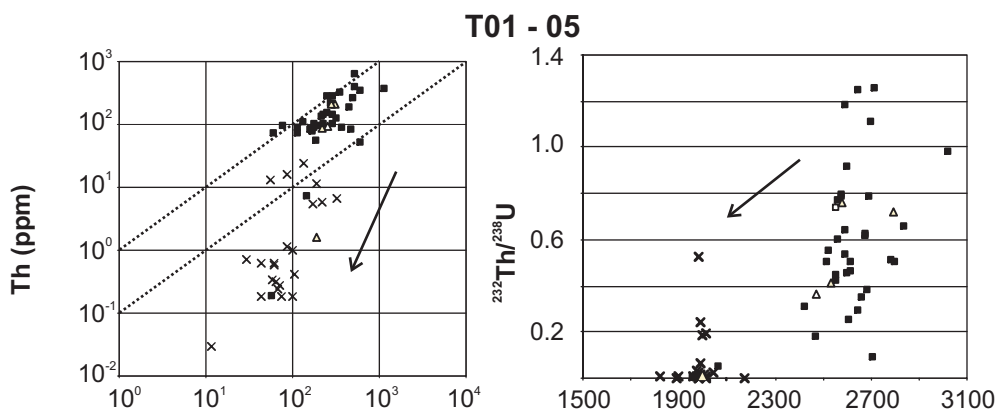
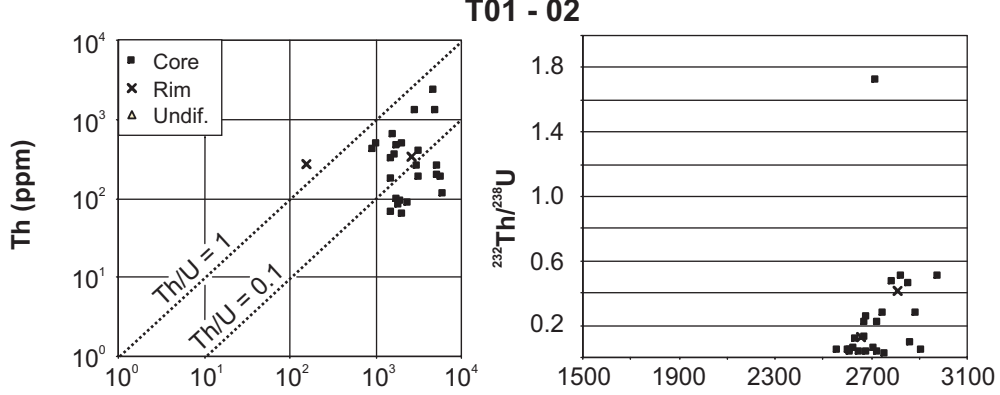












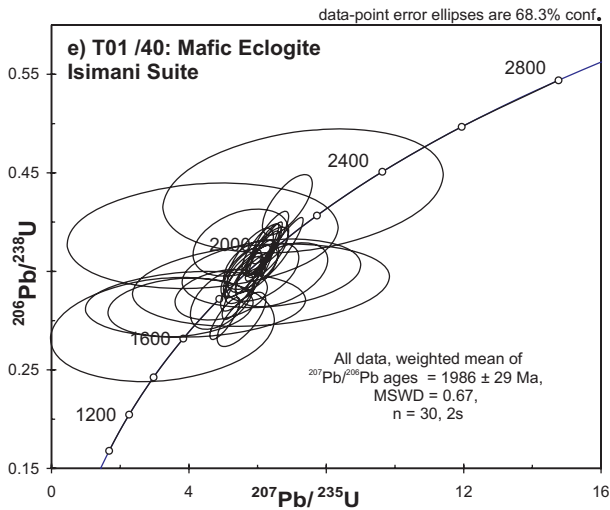
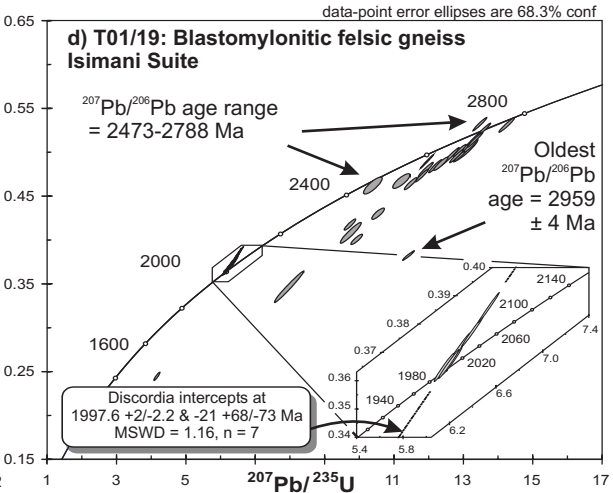
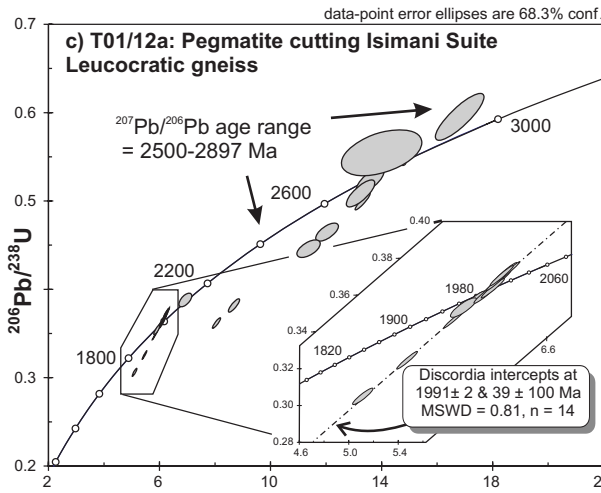
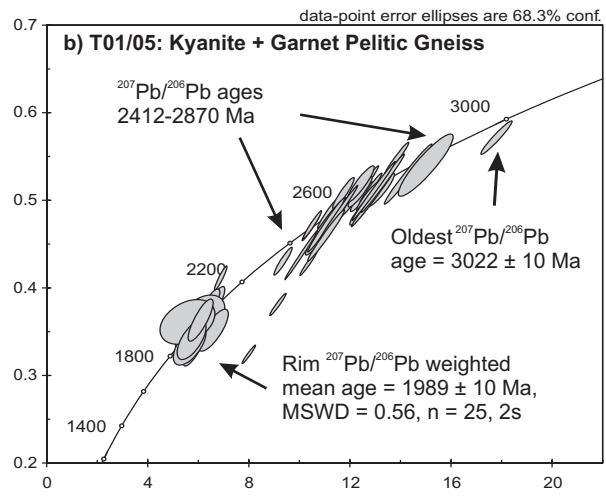
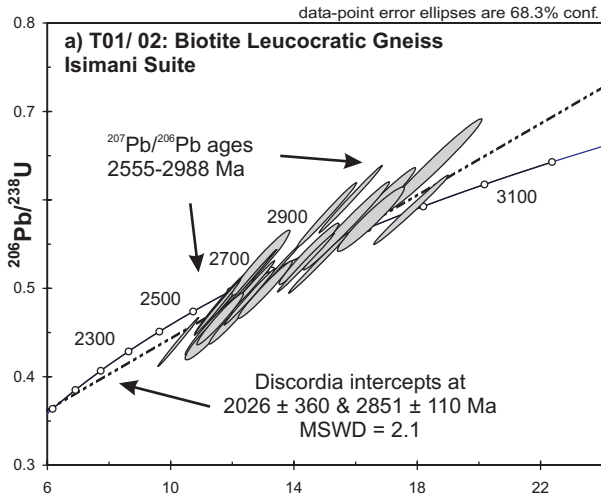


Table 1

Samples run on the SHRIMP II based at the John de Laeter Centre for Excellence in Mass Spectrometry in Perth, Australia
Common Pb derived from measured ^{204}Pb and assuming a Broken Hill Pb isotopic ratio

Spot name	Spot type	Conc. (ppm)						Ages								
		U	Th	$^{232}\text{Th}/^{238}\text{U}$	%com. ^{206}Pb	$^{206}\text{Pb}^2/^{238}\text{U}$	\pm^3	$^{207}\text{Pb}^2/^{235}\text{U}$	\pm^3	$^{207}\text{Pb}^2/^{206}\text{Pb}$	\pm^3	$^{206}\text{Pb}^2/^{238}\text{U}$	\pm^3	$^{207}\text{Pb}^2/^{206}\text{Pb}$	\pm^3	% disconc.
<i>T01-02</i>																
T02-01.1	c	1768	99	0.06	0.04	0.4964	4.2105	12.1477	4.2179	0.1775	0.2492	2599	90	2629	4	1
T02-02.2	c	1597	646	0.42	0.05	0.5182	4.1767	13.4093	4.1837	0.1877	0.2430	2691	92	2722	4	1
T02-03.1	r	158	264	1.73	0.48	0.4557	4.8859	11.3629	5.0262	0.1809	1.1793	2420	99	2661	20	10
T02-03.2	c	1891	84	0.05	0.37	0.4373	4.1824	10.2683	4.2002	0.1703	0.3856	2339	82	2561	6	9
T02-04.1	c	3109	263	0.09	0.03	0.5915	4.9636	16.6843	5.0569	0.2046	0.9672	2995	119	2863	16	-4
T02-05.1	c	3212	405	0.13	0.22	0.4812	4.2774	12.0949	4.3033	0.1823	0.4707	2533	90	2674	8	6
T02-06.1	c	4700	2307	0.51	0.12	0.5695	5.7997	15.7045	5.8653	0.2000	0.8747	2906	136	2826	14	-3
T02-07.1	c	2417	89	0.04	0.09	0.4842	4.4657	11.7329	4.5375	0.1758	0.8040	2545	94	2613	13	3
T02-08.1	c	1557	178	0.12	0.05	0.5274	4.6183	12.9458	4.7713	0.1780	1.1986	2731	103	2635	20	-4
T02-09.1	c	2012	497	0.26	0.04	0.4987	4.1760	12.5819	4.2060	0.1830	0.5014	2608	90	2680	8	3
T02-10.1	c	5140	195	0.04	0.05	0.5096	4.3115	12.6187	4.3179	0.1796	0.2342	2655	94	2649	4	0
T02-10.2	c	1551	68	0.05	0.05	0.4787	4.1852	11.5565	4.2008	0.1751	0.3615	2522	87	2607	6	3
T02-11.1	c	1927	92	0.05	0.41	0.4764	4.2836	11.5251	4.3022	0.1755	0.4006	2511	89	2610	7	4
T02-12.1	c	6022	118	0.02	0.02	0.6000	4.2398	15.8470	4.2611	0.1916	0.4248	3030	102	2756	7	-9
T02-12.2	c	5672	187	0.03	0.02	0.5819	4.1674	15.0847	4.2049	0.1880	0.5603	2957	99	2725	9	-8
T02-12.3	c	5299	256	0.05	0.07	0.6388	5.4280	18.5494	5.5227	0.2106	1.0182	3184	136	2910	16	-9
T02-13.1	c	2058	63	0.03	0.05	0.4451	4.1799	11.2502	4.4769	0.1833	1.6034	2373	83	2683	27	13
T02-14.1	c	1527	315	0.21	1.07	0.4649	4.2047	12.0397	4.3010	0.1878	0.9049	2461	86	2723	15	11
T02-15.1	c	1729	455	0.27	0.05	0.4966	4.3526	13.0764	4.4587	0.1910	0.9668	2599	93	2750	16	6
T02-16.1	c	1018	501	0.51	0.32	0.5878	4.4257	17.8111	4.4633	0.2198	0.5786	2981	106	2979	9	0
T02-17.1	c	2918	1326	0.47	0.28	0.5379	4.2850	14.4996	4.3930	0.1955	0.9681	2775	97	2789	16	1
T02-18.1	c	3241	190	0.06	0.08	0.4884	4.2988	12.5606	4.3297	0.1865	0.5164	2564	91	2712	9	6
T02-19.1	c	4892	1324	0.28	0.14	0.5771	4.1975	16.5031	4.3743	0.2074	1.2312	2937	99	2885	20	-2
T02-20.1	c	1665	352	0.22	0.35	0.4636	4.1798	11.6274	4.3042	0.1819	1.0274	2455	85	2670	17	9
T02-21.1	c	946	422	0.46	0.44	0.5271	4.3008	14.8070	4.3245	0.2037	0.4519	2729	96	2856	7	5
T02-22.1	r	2615	330	0.13	0.22	0.5279	4.1864	14.3998	4.2074	0.1978	0.4203	2733	93	2808	7	3
<i>T01-05</i>																
T05-01.1	r	12	0	0.00	1.51	0.3468	3.8219	5.5202	5.5943	0.1154	4.0853	1919	63	1887	74	-2

T05-01.2	r	29	1	0.03	0.08	0.3825	3.0508	6.6394	3.8024	0.1259	2.2695	2088	54	2041	40	-2
T05-01.3	c	301	214	0.73	0.10	0.4865	2.1922	11.4087	2.2408	0.1701	0.4638	2555	46	2559	8	0
T05-02.1	r	218	6	0.03	0.03	0.3674	2.2305	6.1762	2.3508	0.1219	0.7425	2017	39	1984	13	-2
T05-02.2	c	187	53	0.29	0.08	0.5031	2.2589	12.4335	2.4390	0.1792	0.9197	2627	49	2646	15	1
T05-02.3	r	168	5	0.03	0.18	0.4098	2.2791	6.8474	2.4436	0.1212	0.8814	2214	43	1974	16	-11
T05-03.1	c	290	140	0.50	0.07	0.5164	2.8598	12.5496	2.9078	0.1763	0.5264	2684	63	2618	9	-2
T05-03.2	r	317	7	0.02	0.09	0.3663	2.2021	6.1629	2.2846	0.1220	0.6084	2012	38	1986	11	-1
T05-04.1	c	476	80	0.17	0.25	0.4678	2.1515	10.4275	2.2018	0.1617	0.4678	2474	44	2473	8	0
T05-04.2	r	75	0	0.00	0.10	0.3812	2.5281	6.5032	2.8527	0.1237	1.3215	2082	45	2011	23	-3
T05-04.3	r	86	16	0.19	0.67	0.3735	2.4729	6.3934	2.9409	0.1241	1.5918	2046	43	2017	28	-1
T05-05.1	c	529	393	0.77	0.22	0.4766	2.1523	11.2102	2.4204	0.1706	1.1073	2512	45	2563	19	2
T05-06.1	c	295	100	0.35	0.11	0.5132	2.2036	12.7914	2.2537	0.1808	0.4724	2670	48	2660	8	0
T05-06.2	r	43	1	0.01	0.72	0.3681	2.8071	6.2112	3.6502	0.1224	2.3333	2020	49	1991	41	-1
T05-07.1	r	88	1	0.01	0.10	0.3716	2.4704	6.3259	2.7577	0.1235	1.2255	2037	43	2007	22	-1
T05-07.2	r	186	11	0.06	0.24	0.3637	2.2950	6.1193	2.4978	0.1220	0.9859	1999	39	1986	18	-1
T05-07.3	c	524	634	1.25	0.24	0.3221	2.1569	7.9531	2.2243	0.1791	0.5432	1800	34	2645	9	47
T05-08.1	c	218	130	0.61	0.09	0.5033	2.2506	12.6988	2.4467	0.1830	0.9598	2628	49	2680	16	2
T05-08.2	r	66	0	0.01	0.58	0.3637	2.6257	6.1265	3.4396	0.1222	2.2218	2000	45	1988	40	-1
T05-09.1	c	78	94	1.25	0.46	0.5107	2.5451	13.1515	2.8253	0.1868	1.2265	2660	55	2714	20	2
T05-09.2	r	61	1	0.01	0.72	0.3648	2.6883	6.0554	3.5964	0.1204	2.3889	2005	46	1962	43	-2
T05-10.1	c	230	142	0.64	0.15	0.3796	2.2438	9.1062	2.3187	0.1740	0.5846	2074	40	2596	10	25
T05-10.2	r	44	0	0.00	1.36	0.3555	2.8490	5.6986	4.6226	0.1162	3.6403	1961	48	1899	65	-3
T05-11.1	c	353	312	0.91	0.07	0.4893	2.1906	11.7847	2.2339	0.1747	0.4376	2568	46	2603	7	1
T05-11.2	r	101	0	0.00	0.53	0.3552	2.4560	5.9572	3.0406	0.1216	1.7926	1960	42	1980	32	1
T05-12.1		256	91	0.37	0.16	0.4713	2.2318	10.4817	2.3070	0.1613	0.5843	2489	46	2469	10	-1
T05-13.1	c	292	276	0.98	0.08	0.5710	2.2157	17.7725	2.3011	0.2257	0.6211	2912	52	3022	10	4
T05-13.2	r	131	24	0.19	0.80	0.3833	2.3954	6.4859	3.2228	0.1227	2.1561	2092	43	1996	38	-5
T05-14.1	c	211	93	0.46	0.21	0.4980	2.2707	11.9936	2.4280	0.1747	0.8597	2605	49	2603	14	0
T05-14.2	r	70	0	0.00	0.66	0.3749	2.6463	6.2965	3.3078	0.1218	1.9845	2052	47	1983	35	-3
T05-15.1	c	458	186	0.42	0.09	0.4696	2.1668	11.0066	2.2160	0.1700	0.4640	2482	45	2558	8	3
T05-16.1	c	179	87	0.50	0.12	0.4835	2.2979	11.0750	2.3839	0.1661	0.6344	2542	48	2519	11	-1
T05-17.1	c	116	89	0.79	0.25	0.4886	2.4205	12.4588	2.5746	0.1849	0.8773	2565	51	2698	14	5
T05-18.1	hom	188	2	0.01	0.10	0.3683	2.2936	6.2245	2.5229	0.1226	1.0509	2021	40	1994	19	-1
T05-19.1	c	165	81	0.50	0.08	0.5437	2.3097	14.7885	2.4004	0.1973	0.6534	2799	52	2804	11	0
T05-20.1		215	86	0.41	0.11	0.5073	2.2877	11.7101	2.4552	0.1674	0.8912	2645	50	2532	15	-4
T05-21.1	c	256	154	0.62	0.08	0.5469	2.2651	13.7988	2.3255	0.1830	0.5262	2812	52	2680	9	-5
T05-21.2	r	106	0	0.00	0.35	0.3697	2.4639	6.3170	2.9441	0.1239	1.6114	2028	43	2014	29	-1
T05-22.1	c	1179	352	0.31	0.05	0.4290	2.4596	9.3056	2.6102	0.1573	0.8738	2301	48	2427	15	5

T05-23.1		313	217	0.72	0.26	0.5343	2.2149	14.4277	2.3124	0.1958	0.6644	2760	50	2792	11	1
T05-24.1	c	175	77	0.46	0.26	0.5089	2.2956	12.3644	2.4969	0.1762	0.9823	2652	50	2617	16	-1
T05-25.1	c	61	70	1.18	0.44	0.5176	2.6635	12.3870	2.9257	0.1736	1.2107	2689	59	2592	20	-4
T05-26.1	c	137	105	0.79	0.09	0.4860	2.3549	11.5382	2.4634	0.1722	0.7231	2553	50	2579	12	1
T05-27.1	c	372	89	0.25	0.09	0.4265	2.1864	10.3196	2.2361	0.1755	0.4688	2290	42	2611	8	14
T05-27.2	r	60	1	0.01	0.76	0.3697	2.6767	6.2034	3.9584	0.1217	2.9162	2028	47	1981	52	-2
T05-28.1	c	278	211	0.78	0.15	0.4770	2.2286	11.3427	2.2948	0.1725	0.5475	2514	46	2582	9	3
T05-29.1	c	178	103	0.60	0.43	0.4685	4.5341	11.0021	4.7546	0.1703	1.4311	2477	93	2561	24	3
T05-30.1	c	145	7	0.05	0.66	0.3306	4.3356	5.8209	5.2330	0.1277	2.9302	1841	69	2066	52	12
T05-31.1	c	58	0	0.00	2.18	0.3645	4.6925	6.0439	10.5376	0.1203	9.4352	2003	81	1960	168	-2
T05-31.2	r	67	0	0.00	0.95	0.3500	4.5654	6.5566	5.9037	0.1359	3.7431	1935	76	2175	65	12
T05-32.1	c	614	329	0.55	0.15	0.4359	4.2037	10.0322	4.2266	0.1669	0.4397	2332	82	2527	7	8
T05-33.1	c	620	51	0.09	0.13	0.5009	4.2176	12.8645	4.2475	0.1863	0.5029	2617	91	2710	8	4
T05-33.2	r	57	13	0.25	1.49	0.3333	4.5906	5.6137	7.6234	0.1221	6.0863	1855	74	1988	108	7
T05-34.1	c	259	277	1.11	0.05	0.5185	4.2494	13.2634	4.2889	0.1855	0.5807	2693	94	2703	10	0
T05-35.1	c	228	98	0.45	0.17	0.4708	4.3972	11.0274	4.4635	0.1699	0.7662	2487	91	2556	13	3
T05-36.1	c	324	120	0.38	0.23	0.5098	4.3903	12.9077	4.4196	0.1836	0.5080	2656	96	2686	8	1
T05-36.2	r	58	0	0.01	2.52	0.3594	4.7156	5.5272	13.0663	0.1115	12.1857	1979	80	1825	221	-8
T05-37.1	c	164	81	0.51	0.49	0.5292	4.2944	14.2699	4.3644	0.1956	0.7785	2738	96	2790	13	2
T05-38.1		279	206	0.76	0.19	0.4848	4.2410	11.5184	4.2718	0.1723	0.5119	2548	89	2580	9	1
T05-39.1	c	497	256	0.53	0.33	0.4585	4.2622	11.0136	4.3353	0.1742	0.7929	2433	86	2599	13	7
T05-39.2	r	166	85	0.53	1.22	0.3387	4.3453	5.6864	6.6628	0.1218	5.0508	1880	71	1982	90	5
T05-40.1	r	98	1	0.01	0.92	0.3615	4.4031	6.0431	5.3849	0.1212	3.1000	1990	75	1974	55	-1
T05-41.1	c	115	73	0.66	0.70	0.5394	4.3717	14.9686	4.8270	0.2013	2.0464	2781	99	2837	33	2

T01-12a

T12a-01.1	c	783	61	0.08	0.25	0.3605	1.0984	8.0695	1.2200	0.1624	0.5309	1984	19	2480	9	25
T12a-01.2	r	3645	161	0.05	0.05	0.3637	0.9731	6.1438	1.0026	0.1225	0.2415	2000	17	1993	4	0
T12a-02.1	c	119	78	0.68	1.02	0.5226	1.7336	13.6019	2.4020	0.1888	1.6625	2710	38	2732	27	1
T12a-02.2	r	3083	161	0.05	0.14	0.3566	0.9821	5.9993	1.0434	0.1220	0.3525	1966	17	1986	6	1
T12a-03.1	hom	3625	163	0.05	0.07	0.3568	0.9796	6.0071	1.0537	0.1221	0.3882	1967	17	1987	7	1
T12a-03.2	hom	5838	331	0.06	0.06	0.3722	0.9657	6.2627	0.9990	0.1220	0.2559	2040	17	1986	5	-3
T12a-04.1	hom	5738	425	0.08	0.29	0.3047	0.9759	5.1131	1.0596	0.1217	0.4128	1715	15	1981	7	16
T12a-05.1	hom	9054	415	0.05	0.04	0.3469	0.9601	5.8529	0.9783	0.1224	0.1882	1920	16	1991	3	4
T12a-06.1	c	526	208	0.41	0.23	0.4989	1.2550	13.3249	1.3643	0.1937	0.5351	2609	27	2774	9	6
T12a-06.2	r	4493	242	0.06	0.04	0.3677	0.9760	6.2121	1.0013	0.1225	0.2239	2019	17	1993	4	-1

T12a-07.1	c	225	57	0.26	1.04	0.4638	1.4739	12.0416	2.2633	0.1883	1.7176	2456	30	2727	28	11
T12a-07.2	r	2938	172	0.06	0.36	0.3531	0.9909	5.9272	1.1737	0.1218	0.6290	1949	17	1982	11	2
T12a-08.1	c	169	17	0.10	1.65	0.5949	2.9369	16.8215	3.4570	0.2051	1.8236	3009	71	2867	30	-5
T12a-08.2	r	3204	129	0.04	0.07	0.3607	0.9797	6.1038	1.0257	0.1227	0.3035	1986	17	1996	5	1
T12a-09.1	c	529	48	0.09	0.77	0.3869	1.3082	6.9374	2.1836	0.1300	1.7483	2109	24	2099	31	0
T12a-09.2	r	4821	235	0.05	0.09	0.3636	0.9719	6.1622	1.0068	0.1229	0.2626	1999	17	1999	5	0
T12a-10.1	r	5207	246	0.05	0.04	0.3675	0.9482	6.1996	0.9688	0.1223	0.1990	2018	16	1991	4	-1
T12a-10.2	c	28	280	10.29	2.86	0.5541	3.0644	14.0078	6.8283	0.1833	6.1020	2842	70	2683	101	-6
T12a-11.1	c	294	46	0.16	0.29	0.3807	1.2895	8.6920	1.5186	0.1656	0.8021	2080	23	2513	13	21
T12a-11.2	r	6999	361	0.05	0.03	0.3727	0.9492	6.2881	0.9659	0.1224	0.1788	2042	17	1991	3	-3
T12a-12.1	c	85	41	0.50	1.22	0.5079	1.9633	13.2452	2.5457	0.1891	1.6205	2648	43	2735	27	3
T12a-13.1	hom	6402	394	0.06	0.17	0.3243	0.9800	5.4709	1.0172	0.1224	0.2726	1811	15	1991	5	10
T12a-14.1	c	232	216	0.96	1.15	0.4452	1.4440	11.3785	2.4667	0.1854	1.9999	2374	29	2701	33	14
T12a-14.2	r	4401	229	0.05	0.06	0.3705	0.9777	6.2335	1.0074	0.1220	0.2430	2032	17	1986	4	-2

T01-19

T19-01.1	c	986	405	0.42	0.08	0.5018	1.7149	13.0409	1.8518	0.1885	0.6988	2622	37	2729	12	4
T19-02.1	c	1129	731	0.67	0.25	0.4069	1.9442	9.7286	2.0690	0.1734	0.7075	2201	36	2591	12	18
T19-03.1	c	256	52	0.21	0.14	0.4162	1.0452	9.7106	1.1416	0.1692	0.4593	2243	20	2550	8	14
T19-04.1	r	323	29	0.09	0.05	0.4834	1.0245	12.1789	1.0698	0.1827	0.3079	2542	22	2678	5	5
T19-04.2	c	743	167	0.23	0.25	0.3810	0.9467	11.3998	0.9780	0.2170	0.2452	2081	17	2959	4	42
T19-05.1	c	806	314	0.40	0.12	0.5016	0.9391	12.8894	0.9845	0.1864	0.2956	2621	20	2710	5	3
T19-05.2	c	680	154	0.23	0.06	0.5316	0.9572	13.4629	0.9823	0.1837	0.2206	2748	21	2686	4	-2
T19-06.1	c	1719	138	0.08	0.06	0.4664	1.1790	11.1949	1.4532	0.1741	0.8495	2468	24	2597	14	5
T19-07.1	r	396	75	0.20	0.13	0.3993	0.9841	9.9037	1.1081	0.1799	0.5094	2166	18	2652	8	22
T19-07.2	c	799	428	0.55	0.11	0.4947	1.3727	12.6042	1.3991	0.1848	0.2708	2591	29	2696	4	4
T19-08.1	r	602	150	0.26	0.03	0.4289	0.9785	10.5214	1.1439	0.1779	0.5926	2301	19	2634	10	14
T19-08.2	c	273	219	0.83	0.95	0.4611	1.4037	10.3720	1.6895	0.1632	0.9402	2444	29	2489	16	2
T19-09.1	c	799	408	0.53	0.13	0.4795	1.1476	11.8956	1.1964	0.1799	0.3383	2525	24	2652	6	5
T19-10.1	c	1086	460	0.44	0.02	0.5254	0.9300	13.5769	0.9544	0.1874	0.2144	2722	21	2720	4	0
T19-11.1	c	579	222	0.40	0.05	0.5150	0.9737	13.3105	0.9995	0.1875	0.2258	2678	21	2720	4	2
T19-11.2	r	1640	28	0.02	0.02	0.3672	0.9202	6.2215	0.9453	0.1229	0.2163	2016	16	1999	4	-1
T19-12.1	r	3110	44	0.01	0.01	0.3744	0.9142	6.3731	0.9243	0.1235	0.1365	2050	16	2007	2	-2
T19-12.2	c	987	1293	1.35	0.22	0.4953	0.9290	12.9017	0.9598	0.1889	0.2413	2593	20	2733	4	5
T19-13.1	r	3397	43	0.01	0.01	0.3718	0.9095	6.2878	0.9201	0.1227	0.1390	2038	16	1995	2	-2
T19-13.2	c	1620	714	0.46	0.02	0.5065	0.9183	13.1875	0.9752	0.1888	0.3284	2642	20	2732	5	3

T19-14.1	c	918	437	0.49	0.12	0.4725	1.0252	11.7871	1.0658	0.1809	0.2912	2495	21	2661	5	7
T19-15.1	r	3530	43	0.01	0.00	0.3648	0.9074	6.1559	0.9272	0.1224	0.1903	2005	16	1992	3	-1
T19-15.2	c	1140	94	0.09	0.38	0.3449	3.4133	7.9405	3.4750	0.1670	0.6522	1910	56	2527	11	32
T19-16.1	hom	3783	50	0.01	0.01	0.3774	0.9434	6.3972	0.9510	0.1229	0.1195	2064	17	1999	2	-3
T19-17.1	c	365	205	0.58	0.04	0.5306	0.9962	14.2505	1.0336	0.1948	0.2755	2744	22	2783	5	1
T19-18.1	hom	5498	71	0.01	0.00	0.3859	0.9068	6.5382	0.9123	0.1229	0.1007	2104	16	1998	2	-5
T19-19.1	c	1667	806	0.50	0.01	0.4888	1.0406	11.9283	1.0492	0.1770	0.1334	2565	22	2625	2	2
T19-20.1	r	4532	564	0.13	0.41	0.2422	1.2954	4.1240	1.3925	0.1235	0.5110	1398	16	2007	9	44
T19-22.1	r	3129	48	0.02	0.06	0.3659	0.9200	6.1936	0.9321	0.1228	0.1494	2010	16	1997	3	-1
T19-22.2	c	269	37	0.14	0.27	0.4863	1.0361	12.3388	1.1154	0.1840	0.4130	2555	22	2689	7	5
T19-23.1	c	506	119	0.24	0.16	0.4633	0.9881	11.4676	1.0565	0.1795	0.3740	2454	20	2648	6	8
T19-24.1	c	1830	806	0.45	0.03	0.5138	1.0932	13.3286	1.1159	0.1881	0.2241	2673	24	2726	4	2
T19-25.1	c	436	87	0.21	0.01	0.4950	0.9970	12.7937	1.0316	0.1875	0.2651	2592	21	2720	4	5

T01-40

T40-01.1	l	75	110	1.53	2.01	0.3529	4.6047	5.8671	8.2534	0.1206	6.8495	1949	77	1965	122	1
T40-02.1	d	6	1	0.24	10.01	0.3362	8.1974	6.1116	40.4463	0.1318	39.6069	1868	133	2123	694	14
T40-02.2	l	10	2	0.21	8.46	0.3133	6.2999	3.7691	37.1102	0.0873	36.5716	1757	97	1366	704	-22
T40-03.1	l	4	1	0.19	12.52	0.2908	11.9903	3.2515	66.2461	0.0811	65.1519	1645	174	1224	1280	-26
T40-04.1	l	7	1	0.21	6.84	0.3481	6.6024	6.4195	26.6978	0.1337	25.8686	1926	110	2148	452	12
T40-05.1	l	40	31	0.81	2.32	0.3568	4.6887	5.8286	9.0790	0.1185	7.7746	1967	79	1933	139	-2
T40-05.2	l	42	25	0.61	1.51	0.3520	4.6250	5.8962	5.6501	0.1215	3.2455	1944	78	1978	58	2
T40-06.1	l	29	18	0.65	1.27	0.3719	4.6825	6.1390	6.2551	0.1197	4.1474	2038	82	1952	74	-4
T40-06.2	d	44	33	0.77	1.87	0.4177	4.8923	6.8852	6.9886	0.1196	4.9906	2250	93	1950	89	-13
T40-07.1	l	42	54	1.33	1.19	0.3656	4.5581	6.1585	5.2884	0.1222	2.6815	2009	79	1988	48	-1
T40-08.1	l	40	17	0.44	0.82	0.3715	4.6950	6.1448	5.2181	0.1199	2.2771	2037	82	1955	41	-4
T40-09.1	l	22	5	0.22	2.47	0.3481	4.7794	5.5479	7.0186	0.1156	5.1399	1926	80	1889	93	-2
T40-09.2	l	24	5	0.23	0.60	0.3741	5.4372	6.7302	5.9581	0.1305	2.4364	2049	95	2105	43	3
T40-15.1	l	28	24	0.90	1.92	0.3414	7.7875	5.7476	8.7841	0.1221	4.0638	1893	128	1987	72	5
T40-10.2	d	12	4	0.35	3.18	0.3491	5.6269	6.1644	11.2160	0.1281	9.7024	1930	94	2072	171	7
T40-11.1	d	7	1	0.20	6.54	0.3792	5.9311	5.5225	16.6416	0.1056	15.5488	2073	105	1725	286	-17
T40-12.1	d	2	1	0.25	16.32	0.3863	9.1302	4.4176	58.8699	0.0829	58.1575	2105	164	1268	1135	-40
T40-13.1	l	41	25	0.63	0.63	0.3733	4.7819	6.2442	5.2055	0.1213	2.0568	2045	84	1976	37	-3
T40-14.1	d	7	2	0.31	4.23	0.3467	6.2011	6.7078	13.2560	0.1403	11.7161	1919	103	2231	203	16
T40-15.1	d	4	1	0.41	12.85	0.4320	9.6132	7.3431	36.6771	0.1233	35.3949	2315	187	2004	628	-13
T40-16.1	d	26	6	0.22	2.46	0.3590	6.4364	5.7454	8.4218	0.1161	5.4314	1978	110	1896	98	-4

T40-16.2	l	30	8	0.28	10.36	0.3164	6.9459	4.2061	50.4112	0.0964	49.9304	1772	108	1556	937	-12
T40-17.1	l	73	81	1.15	1.06	0.3021	4.6461	5.0674	5.6498	0.1217	3.2147	1702	69	1981	57	16
T40-18.1	l	55	72	1.34	2.51	0.3694	4.6005	6.2897	6.4324	0.1235	4.4958	2026	80	2007	80	-1
T40-19.1	d	42	43	1.06	2.47	0.3413	4.6870	5.6581	6.8588	0.1202	5.0076	1893	77	1960	89	4
T40-20.1	d	63	93	1.53	1.46	0.3845	4.5868	6.3734	5.6262	0.1202	3.2581	2097	82	1960	58	-7
T40-21.1	d	30	6	0.21	1.53	0.3013	6.0565	5.5469	8.4434	0.1335	5.8831	1698	90	2145	103	26
T40-21.2	l	30	7	0.24	1.89	0.3390	5.7110	5.5550	7.4221	0.1188	4.7404	1882	93	1939	85	3
T40-22.1	l	27	9	0.34	4.31	0.3262	5.1706	4.9565	17.9336	0.1102	17.1720	1820	82	1803	312	-1
T40-23.1	l	43	35	0.84	2.90	0.3217	6.2399	4.9845	12.2336	0.1124	10.5227	1798	98	1838	191	2

²radiogenic Pb only ³all errors are absolute, 1s errors

Table 2

Spot name	U (ppm)	Th (ppm)	$^{232}\text{Th}/^{238}\text{U}$	$^{207}\text{Pb}/^{206}\text{Pb}$ Age (Ma)	\pm (Ma)	Ln (UO/U)	Ln (Pb/U)	
<i>All T02.xx</i>								
cz3.1	608	31	0.05	539.05	4.24	1.9042	-1.5734	Calculated 2 sigma external spot-to-spot error = 8.32% no rejections
cz3.2	605	32	0.05	563.41	6.23	1.8866	-1.5818	
cz3.3	625	32	0.05	571.42	5.27	1.8564	-1.6430	
cz3.4	604	31	0.05	586.98	13.11	1.8702	-1.5781	
cz3.5	620	32	0.05	531.15	5.72	1.8582	-1.6847	
cz3.6	582	30	0.05	544.04	10.66	1.8548	-1.6930	
cz3.7	603	31	0.05	575.79	15.83	1.8900	-1.5397	
cz3.8	575	30	0.05	553.95	3.98	1.8787	-1.6090	
cz3.9	583	30	0.05	572.71	8.78	1.8489	-1.6616	
cz3.10	621	32	0.05	603.96	4.48	1.8524	-1.5989	
cz3.11	584	30	0.05	542.24	8.54	1.7486	-1.9617	
cz3.12	591	31	0.05	586.92	3.99	1.8925	-1.5266	
<i>T05-01.1 to T05-28.1</i>								
cz3.1	493	25	0.05	557.19	3.81	1.6921	-2.0134	Calculated 2 sigma external spot-to-spot error = 4.17% no rejections
cz3.2	578	30	0.05	570.40	3.23	1.7606	-1.8140	
cz3.3	620	32	0.05	560.56	5.57	1.7762	-1.7923	
cz3.4	606	31	0.05	568.95	6.87	1.7649	-1.8066	
cz3.5	589	30	0.05	542.24	3.63	1.6727	-2.0814	
cz3.6	603	31	0.05	569.92	3.38	1.7820	-1.7618	
cz3.7	605	31	0.05	581.48	3.51	1.7771	-1.7556	
cz3.8	606	31	0.05	569.32	3.42	1.8023	-1.7124	
cz3.9	598	31	0.05	563.48	3.78	1.8092	-1.7011	
cz3.10	609	31	0.05	559.17	8.55	1.7876	-1.7652	
cz3.11	591	30	0.05	576.77	3.79	1.7748	-1.7733	
cz3.12	592.7	30.46	0.05	546.72	4.20	1.8091	-1.7386	
<i>T05-29.1 to T05-41.1</i>								
cz3.1	608	31	0.05	539.05	4.24	1.9042	-1.5734	Calculated 2 sigma external spot-to-spot error = 8.32%
cz3.2	605	32	0.05	563.41	6.23	1.8866	-1.5818	

cz3.3	625	32	0.05	571.42	5.27	1.8564	-1.6430
cz3.4	604	31	0.05	586.98	13.11	1.8702	-1.5781
cz3.5	620	32	0.05	531.15	5.72	1.8582	-1.6847
cz3-6	582	30	0.05	544.04	10.66	1.8548	-1.6930
cz3.7	603	31	0.05	575.79	15.83	1.8900	-1.5397
cz3.8	575	30	0.05	553.95	3.98	1.8787	-1.6090
cz3.9	583	30	0.05	572.71	8.78	1.8489	-1.6616
cz3.10	621	32	0.05	603.96	4.48	1.8524	-1.5989
cz3.11	584	30	0.05	542.24	8.54	1.7486	-1.9617
cz3.12	591	31	0.05	586.92	3.99	1.8925	-1.5266

no rejections

All T012a.xx

cz3.1	596	31	0.05	575.77	5.99	1.8663	-1.6302
cz3.2	599	31	0.05	562.66	4.79	1.8607	-1.6668
cz3.3	607	32	0.05	558.13	3.15	1.8514	-1.7000
cz3.4	577	30	0.05	565.63	6.98	1.8524	-1.6853
cz3.5	598	31	0.05	571.92	4.80	1.8269	-1.7356
cz3.6	603	32	0.05	560.28	4.90	1.8569	-1.6813
cz3.7	626	32	0.05	571.05	4.85	1.8457	-1.6967
cz3.8	627	33	0.05	562.21	6.72	1.8468	-1.7135
cz3.9	609	32	0.05	556.23	7.08	1.8703	-1.6529
cz3.10	579	30	0.05	556.00	4.39	1.8359	-1.7430
cz3.11	576	30	0.05	533.25	5.57	1.8956	-1.6292
cz3.12	582	30	0.05	560.03	4.73	1.8014	-1.8293
cz3.13	623	33	0.06	575.15	6.87	1.8763	-1.5966

Calculated 2 sigma external spot-to-spot error = 1.69%

cz3.11 rejected

All T19.xx

cz3.01	506	26	0.05	584.98	2.31	1.6496	-2.0533
cz3.02	598	30	0.05	560.49	2.24	1.6794	-2.0150
cz3.03	611	31	0.05	563.70	2.73	1.7293	-1.8779
cz3.04	574	29	0.05	563.23	2.76	1.6520	-2.0714
cz3.05	617	32	0.05	571.05	2.31	1.6987	-1.9475
cz3.06	647	33	0.05	563.90	3.42	1.7478	-1.8391
cz3.07	618	32	0.05	572.98	3.51	1.6999	-1.9416
cz3.08	649	33	0.05	564.76	2.29	1.7272	-1.8870
cz3.09	576	29	0.05	554.82	2.48	1.6829	-2.0246
cz3.10	582	30	0.05	560.82	6.20	1.6971	-1.9737

Calculated 2 sigma external spot-to-spot error = 1.79%

cz3.01 rejected

All T40.xx

cz3.01	565	22	0.04	551.42	4.05	1.8469	-1.5781
cz3.02	613	25	0.04	515.59	3.05	1.8218	-1.6940
cz3.03	588	24	0.04	543.21	15.31	1.9023	-1.5708
cz3.05	644	26	0.04	581.02	3.96	1.7312	-1.7633
cz3.06	633	26	0.04	575.64	2.87	1.7729	-1.6820
cz3.07	667	27	0.04	554.20	3.42	1.7737	-1.7114
cz3.08	541	22	0.04	547.69	2.35	1.7247	-1.8314
cz3.09	592	24	0.04	585.29	8.41	1.7313	-1.7480
cz3.10	607	25	0.04	588.03	3.44	1.7461	-1.7051
cz3.11	580	23	0.04	593.98	5.51	1.7427	-1.7086
cz3.12	576	23	0.04	565.05	5.77	1.7475	-1.7603

Calculated 2 sigma external spot-to-spot error = 8.74%

no rejections